

Comparative field study of shallow rhyolite intrusions in Iceland: emplacement mechanisms and impact on country rocks

Elodie Saubin¹, Ben Kennedy¹, Hugh Tuffen², Marlene Villeneuve¹, Jonathan Davidson¹, Steffi Burchardt³

¹ Department of Geological Sciences, University of Canterbury, Ilam road, Christchurch 8041, New Zealand

² Lancaster Environment Centre, Lancaster University, Lancaster, UK

³ Department of Earth Science, Uppsala University, Uppsala, Sweden

Corresponding author: elodie.saubin@pg.canterbury.ac.nz

Declarations of interest: none

Keywords: Rhyolite. Intrusion. Iceland. Damage. Emplacement. Permeability

Abstract

Shallow silicic intrusions are known to exist in many active volcanoes and can fuel both eruptions and hydrothermal fields. However, our knowledge of magma intrusions remains far from complete, and processes occurring at intrusion margins are poorly understood. In this field-based study, we characterise four shallow, dissected rhyolitic intrusions at three sites in Iceland (Njarðvík-Dyrfjöll, Krafla and Húsafell central volcanoes). We focus on the relationship between intrusion emplacement mechanisms and country rock response, employing scanline mapping of fractures and in-situ rock property measurements (hardness and permeability) along transects from the intrusion margins to damaged and undamaged country rocks.

We identify various scenarios of shallow intrusion emplacement style, based upon their diverse geometry and lithofacies architecture. Additional information, which is gained from rock properties and characteristics of populations of fractures and vesicles, indicates that initial country rock properties strongly influence the emplacement style. We expect that our results are representative for active hydrothermal systems lying above the crustal brittle/ductile transition. Two discrete types of country rock response to magma injection are identified. The matrix permeability of weak, porous and permeable lithologies (conglomerate and hyaloclastite) is

reduced by >1 order of magnitude adjacent to intrusions due to pore occlusion, although bulk permeability could be affected by increased fracturing. In contrast, stronger and denser, low-permeability lithologies (basalt and welded ignimbrite) undergo a decrease in hardness by a factor >2, related to an up to fivefold increase in fracture density.

1. Introduction

Magmatic activity in Iceland is dominantly basaltic in composition (Walker, 1966; Sigurdsson, 1977; Thordarson and Larsen, 2007). However, rhyolitic magma is generated at central volcanoes by partial melting of altered basaltic crust and/or fractional crystallisation (e.g. Jónasson, 1994; Gunnarsson et al., 1998). The silicic magma produced moves through the crust along multiple fracture networks in the country rock (e.g. Walker, 1974; Spence and Turcotte, 1985; Senger et al., 2014). This magma eventually accumulates in the shallow crust, solidifying to produce rhyolitic intrusions or erupting as lavas or pyroclastic deposits (e.g. Walker; 1974; Burchardt et al., 2012, Weidendorfer et al., 2014). Rhyolitic intrusive complexes become the shallow roots of some of the most vigorous hydrothermal systems, used for geothermal energy production in Iceland (e.g. Krafla), which is already one of the largest producers of geothermal energy worldwide (Nielsen et al, 2000; Arnorsson et al, 2008). Rock properties at the margins of the intrusions, including permeability, likely control both eruption and energy potential (e.g. Lamur et al., 2017, Eggertsson et al., 2018, Mordensky et al., 2018a and b). These conditions are of major importance for both drilling and extraction in a suitable and efficient way, which can be developed into a more powerful source of energy when supercritical fluids are reached (40-50 MWe per well; Albertsson et al., 2003). However, active rhyolitic intrusions are difficult to geophysically identify in the subsurface beneath active volcanoes, and hydrothermal systems may mask their presence (e.g. Elders et al., 2011). It is therefore important to elucidate details about the defining physical properties of intrusions and their surrounding rocks and hydrothermal system.

Processes related to magma transport in volcanic plumbing systems are the subject of active research (Burchardt, 2018), illustrated in recent studies reviewing melt segregation, emplacement and storage systems (e.g. Holness, 2018; Healy et al., 2018). Magma emplacement style depends on physical properties and structure of surrounding rocks, and regional tectonics (Pollard, 1973; Spence and Turcotte, 1985; Hutton, 1988; Clemens and Petford, 1999; Galland et al., 2006). A transition from a dyke to a sill could for instance be associated to a variation of strength in layered country rocks (Kavanagh et al. 2006; Maccaferri et al., 2011) and/or to the occurrence of a strong compressive tectonic stress (Gudmundsson., 1990; Maccaferri et al., 2011). The country rock lithology can affect the intrusion width (Krumbholz et al. 2014), as well as

magma viscosity, but has been postulated to have little effect on the emplacement style (e.g. Clemens and Petford, 1999, Mathieu et al., 2008). Propagating magma exploits pre-existing discontinuities in country rock (Lamur et al., 2017; Le Corvec et al., 2013), but also creates new fractures. The end-member mechanisms of country rock failure are (1) hydraulic tensile fracturing in shallow cohesive environments at thin intrusive tips and (2) shear faulting in low cohesive rocks affected by a broad intrusive tip (Mathieu et al., 2008). The opening direction of intrusions is therefore a result of stresses and country-rocks properties, and is parallel to the minimum compressive stress (Kavanagh, 2018). These fracturing processes include the formation of tuffisite veins, which open pathways for silicic magma to propagate, degas, and erupt (e.g. Stasiuk et al., 1996; Tuffen and Dingwell, 2005; Saubin et al., 2016). They form by exsolved magmatic gas that inject into fractures within country rocks (Heiken et al., 1988). The gas flow carries particles of magma and country rock, resulting in complex sedimentary structures (Stasiuk et al., 1996; Tuffen and Dingwell, 2005). Continued propagation of pressurised magmatic fluids can widen the veins, facilitating magma emplacement (McGowan, 2016), and magma intruded along the fracture network deforms and cools whilst simultaneously heating the country rock.

Besides fracturing occurring at the intrusive tips, country rocks can be locally deformed and fractured along the contacts (Kavanagh and Sparks, 2011). In shallow environments, this damage mostly results from compressive and shear stresses exerted by intrusive magma on country rocks (e.g. Mattsson et al., 2018; Galland et al., 2009). Strong, low-porosity material undergoes limited elastic or inelastic deformation response to pressure increase associated with intrusion, leading to material failure (e.g. Paterson et al., 1996). In contrast, weak, highly-porous units such as sedimentary rocks favour the circulation of hot fluids and will undergo significant ductile deformation with shear failure (Wong and Baud, 2012; Mordensky et al., 2019). They are consequently more prone to thermal alteration and thermal fracturing (e.g. Delaney et al., 1986). Within the intrusion, orientation of cooling fractures strongly depends on the intrusive geometry (Senger et al., 2014), and smaller-scale (millimetre) perlitic fracture networks can develop in quenched glassy margins (von Aulock et al., 2013), facilitating significant ingress of external water. In the country rock at the immediate vicinity of the intrusion, the high fracture density caused by brittle deformation and thermal cracking, associated with permeability increase, allows circulation of high-enthalpy fluids (e.g. Carrigan; 1986; Paterson et al., 1996; Scott et al., 2017; Mordensky et al., 2018a, 2018b). Fractures propagating further into the country rock will become increasingly influenced by tectonic forces and pre-existing fracture populations (Senger et al., 2014) and may create conditions suitable for a geothermal resource.

Magma propagation and country rock response elucidate textural, as well as structural adjustments. For instance, high internal shear stress and rapid quenching at the contact can form

platy jointing (Conway et al., 2015; Magnall et al., 2018). Decompression of ascending magma causes melt to degas through vesicle nucleation and growth (e.g. Hamada et al., 2010). Parameters impacting this magma response include the decompression rate, magma viscosity, its volatile content and quenching rate (e.g. Sparks, 1978; Papale et al., 1998; Shea et al., 2010 *and references therein*; von Aulock et al., 2017). The melt flow deforms vesicles according to the strain rate, which changes depending on the velocity gradient across the intrusion (e.g. Rust et al., 2003; Okumura et al., 2009; Dingwell et al., 2016). Secondary changes may be caused by coalescence, outgassing or relaxation, and a pumiceous foam can form for highly-vesicular magma, then fragment or collapse (Westrich et al., 1988; Okumura et al., 2006; Kennedy et al., 2016). Vesicle size distribution can consequently be an indicator of degassing processes, and vesicle shapes and orientations can record processes related to stress and flow direction (e.g. Sparks, 1978; Stasiuk et al., 1996; Manga et al., 1998; Shea et al., 2010; Toramaru, 2014; Wadsworth et al., 2017, Dingwell et al., 2016). Besides vesiculation, crystallisation may occur during slow cooling, but is dominated by subsolidus crystallisation and spherulite formation in narrow, rapidly-quenched rhyolite bodies (von Aulock et al., 2013).

Magma emplacement also affects the country rock composition. Hydrothermal alteration of rocks at the interface depends on temperature and diffusivity contrast, the presence of fluids, initial materials chemistry and pre-existing structures (e.g. Alt et al., 1986; Pirajino, 2008; Annen, 2017). Heat conduction can be associated with heat convection or advection by hydrothermal fluids in presence of a developed fracture network (e.g. Parmentier and Schedl, 1981; Huppert et Sparks, 1989). Hot aqueous fluids drive mineralogical, chemical and textural changes in the rock, with released oxygen causing oxidation and thus colour change, together with iron leaching (e.g. Pirajino, 2008). In addition, the heat can dehydrate mineral species in the country rock, dissolving incompatible chemical species that precipitate as secondary minerals (e.g. Galushkin, 1997; Siratovich et al., 2011). Despite the importance of these processes in country rock alteration, chemical impacts of intrusions are beyond the scope of this study.

This paper uses field case studies of four fossil rhyolitic intrusions from three plumbing systems, which are analogues to shallow active systems in Iceland, to investigate the relationships between intrusion processes and country rocks, and their effects on the resulting rock mass permeability associated with the intrusion. We characterise a variety of country rocks to examine the effects of intrusion on different rock types. Vesicle populations within intrusions records cooling and emplacement processes, and field estimates of rock hardness, permeability and fracture density indicate the mechanical and thermal impacts of rhyolite intrusion at the country rock interface. We use these field observations and measurements, as well as interpretations of intrusive processes to conceptualise the influence of the country rock and intrusion style on the

emplacement, degassing, and geothermal potential of rock masses surrounding shallow rhyolite intrusions.

2. Methodology

The field areas (Fig. 1) all comprise one or more shallow rhyolite body, intruded within diverse country rock lithologies. These sites were chosen to represent similar intrusion compositions, dimensions and emplacement depths, at relatively unweathered and accessible outcrops. Each site was divided into the intrusion, the damaged zone in the country rock and the undamaged country rock. The term “damaged zone” in this study refers to both hydrothermal alteration and intrusion-triggered mechanical damage. We conducted qualitative and quantitative assessment of intrusion dimensions, geometries, and vesicle populations including density, size and orientation. Information collected included the lithofacies architecture, rock properties including hardness and permeability, and details of fracture populations including density, size and orientation primarily in the country rock damaged zone, but also in the undamaged country rock away from the intrusion as a control. Additional features such as tuffisite veins and brecciated zones are also included in the descriptions. Figure S1 (Supplemental Material) shows the measurement locations.

2.1 3D photogrammetric reconstruction

Models of the three field areas were constructed from photography using the structure from motion (SfM) photogrammetric technique in the Agisoft Photoscan (Metashape) software. Images were collected using either an unmanned aerial vehicle (UAV; DJI phantom 3), or a combination of both the UAV and a handheld camera. The UAV photographs were geo-tagged using a standard GPS, and the final models have an RMS error between the reported and final photo locations on the order of ~3m, over distances as large as several kilometres. The resulting 3D models and orthomosaics were of high resolution, at ~10 mm/pixel, and used to approximate three dimensional intrusion geometries. Orientations of contacts and faults were measured with a compass clinometer in the field, constraining results obtained using the 3D models. Compass measurements were corrected with 10° of declination at Njarðvík-Dyrfjöll (Landsendi outcrop), 11° at Krafla (Hrafninnuhryggur outcrop) and 13° at Húsafell (West and East outcrops), appropriate for the date of fieldwork in 2017 and 2018. Three dimensional intrusive shapes for Figs. 2, 3 and 4 were drafted using structural data gathered from photogrammetric reconstructions.

2.2 Rock properties

Permeability and hardness can be estimated in the field with the respective use of TinyPerm (Farquharson et al., 2015) and Schmidt hammer (Aydin and Basu, 2005). Although such field techniques lack the accuracy of equivalent laboratory measurements, they permit collection of large in-situ datasets, and can be used to reflect relative spatial variation within the outcrop (Mordensky et al., 2018b).

The TinyPerm is a portable air permeameter used perpendicularly to smooth surfaces, that we also placed parallel to vesicle elongation in vesicular rocks. Air is drawn through the volume of rock adjacent to the nozzle, with a vacuum initially created at the nozzle-rock interface (Mordensky et al., 2018b). The permeability calculation used by the TinyPerm is described in Brown and Smith (2013). Trends in permeability within and in between outcrops are considered valid although absolute values should be considered as approximate, with uncertainties of a factor of $\pm 5\%$ (Brown and Smith, 2013). The use of the TinyPerm is validated by laboratory measurements of permeability on a heterogeneous block of hyaloclastite from the field site of Krafla (Fig. 1), which provided the same range of relative values to the field permeameter results, with natural variability of half an order of magnitude (Eggertson et al., 2018). We differentiate in this paper between the matrix permeability measured with the TinyPerm and the rock mass permeability, which takes into account fractures and other lithological structures.

Field rock hardness was determined using a type-L Schmidt hammer, designed for weak rocks (<60 MPa) and requiring a minimum of 10 measurements at each location (ASTM, 2001). The final value is calculated from the average, as suggested in Amaral et al. (1999). The inbuilt spring-driven piston is released on a rock surface, and the rebound is registered. A correlation chart can relate the rebound value to rock strength, depending on hammer orientation (horizontal or vertical; e.g. Deere and Miller, 1966; del Potro and Hürlimann, 2008; Mordensky et al., 2018b), however the absolute values of strength are not well constrained for these rocks. We, therefore, use the rock hardness measurements to assess relative spatial variation of hardness/strength only. Laboratory measurements of Uniaxial Compressive Strength (UCS) were performed by Eggertson (2019) on two Icelandic rocks (dense basalt lava and hyaloclastite) among the four we encounter in this study. Comparing these laboratory values with the rebound values measured on the field, we can consistently estimate the UCS for the two other types of country rocks (conglomerate and welded ignimbrite). A rebound value ~ 35 in our undamaged basalt lava corresponds to an average UCS of 90 MPa (Eggertson, 2019). The rebound value of ~ 45 in welded ignimbrite therefore suits for UCS of 115 MPa.

Field conditions (outcrop quality, dimensions and accessibility) were highly variable and despite efforts made to conduct consistent measurements, inter-site fluctuations were unavoidable. Measurements were recorded over two field seasons and the large number of scientists involved also impacts the consistency in number of measurements. Systematic measurements at ~5-10 cm intervals of rock properties were conducted along 1-4 m long transects, and a subset of them meet our need for results recorded perpendicularly to the contact in representative damage area: 2 transects out of the 5 from Landsendi, 3 out of the 9 from Hrafninnuhryggur 2 out from the 4 at Húsafell West, and the 2 from Húsafell East. Measurements were made on smooth surfaces free from water and lichen, avoiding macro-fractures. At each point, 1-6 good TinyPerm measurements (with smooth temporal decay of pressure differential) were recorded depending on time allocated per outcrop. We aimed for ~10 Schmidt hammer measurements at the same measurement points as the TinyPerm. As Schmidt hammer rebound can damage the rock, permeability was measured first, and each rebound was conducted on a slightly different but adjacent surface. Results presented herein are calculated from the average of measurements for each point.

Del Potro and Hurliman (2008) illustrate the importance of a global standard classification for volcanic rock using an engineering geology approach. They proposed the Geotechnical Classification of Volcanic Material procedure (GCVM), adopted by several authors afterwards (e.g. Mordensky et al., 2018a, 2018b) and based on rock properties of units including their alteration degree (rock texture and composition) that we couple with damage degree (lithological structure). Initially used for characterisation of material stability, it is also strongly related to drillability and relevant for geothermal. We therefore use the GCVM adapted to our field units.

2.3 Fractures

Our approach limits the permeability measurements to the rock matrix, as we intentionally avoided visible fractures. It is therefore important to measure the spacing and dimensions of such discontinuities, in order to consider rock mass permeability. To achieve this, we conducted 1D fracture mapping using scanlines for a systematic record of fracture locations and conditions. Because of the restricted time available to conduct the fieldwork, we followed the quickest simple scanline method in Manda and Mabee (2010). Scanline transects were typically 1-2 m in length, located in each lithology and across the contact in representative areas, and we aimed for >25 counted fractures. Measurements concerned all discontinuity types (joints, bedding, faults, veins) and include orientation, length and aperture, together with additional geometry factors and external effects (results can be made available on request). We used the scanlines to calculate average fracture density (number of fractures per metre) and average fracture area (length multiplied by aperture) for each country rock lithology.

We use a subset of the scanline results that meet our need for a clear distinction between country rock damaged by the intrusion and non-damaged rock: 1 scanline out of the 6 from Landsendi, 3 out of the 11 from Hrafninnuhryggur, 2 out of the 4 from Húsafell West and the 2 from Húsafell East. At Landsendi we used photos taken by a handheld camera at resolution of 1 mm/pixel to record fracture distribution, lengths and apertures along two additional transects, in locations inaccessible in the field. In order to obtain higher resolution information on fracture density at Húsafell West, where the country rock is good quality and smooth, we also counted the number of fractures over a 50 cm length parallel to the contact, repeating the measurement every 5-10 cm along the scanline transects. At Húsafell East, we used the two scanlines and 6 photo-based transects to create a similar high-resolution fracture density profile (c.f. Supplemental Material, Fig.S1, Table S2).

2.4 Textures

Vesicularity was estimated every ~2 m along the outcrop at Landsendi, using a vesicularity reference chart. The orientation, elongation and width of the biggest-sized vesicles were recorded at each outcrop every ~2-5 m along the intrusion, at the core, sill tips, top and bottom contacts, and near features such as faults or internal rock deformation, as well as along profiles across the intrusions. Attempts were made to consider the short and long axes of vesicles in 3 dimensions, but the outcrop surfaces restricted this approach. It is therefore more realistic to consider results as representing 2D vesicles. Vesicle dimensions were measured with a mm-precision scale, resulting in small dimensions to be estimated with a precision of 0.5 mm. Data allowed the calculation of the vesicles' equivalent diameter (i.e. diameter of the rounded-shape vesicle of same area) and shape ratio (short axis divided by long axis). Variation of these parameters for vesicles along profiles will be presented for Húsafell West only, as there are no significant trends at the other field sites.

2.5 Statistical testing

We use the method of one-way analysis of variance (ANOVA; Fisher, 1925) to determine the significance of trends when those are unclear. It is the case for our permeability results, which variations within damaged country rocks are compared with variations in the undamaged rocks. The calculation compares the means of the two groups, taking into account their variance and resulting in an overall p-value (Miller and Rupert, 1997). The two groups are considered significantly different within the 95 % confidence interval when p-value <0.05. If p-value >0.05, the difference is not statistically significant. The data analysis for this study was generated using the Real Statistics Resource Pack software (Zaiontz, 2018).

3. Geological setting and description of intrusions

The three selected central volcanoes in Iceland are Njarðvík-Dyrfjöll, Krafla and Húsafell (Figure 1).

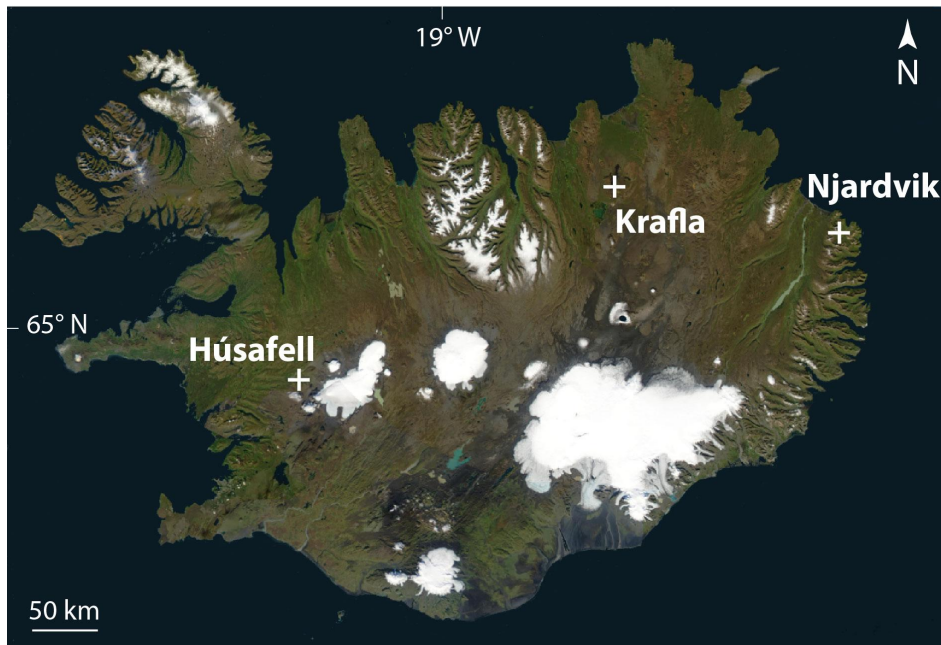


Figure 1. Map of central volcano field areas in Iceland (image from NASA). Refer to Table 1 for the outcrop coordinates.

3.1 Njarðvík-Dyrfjöll

The ~12 Ma Neogene Njarðvík-Dyrfjöll volcano in the East Fjörds hosts an extensive system of rhyolitic dykes and sills. At the base of the edifice is a >300m thick sub-volcanic rhyolitic body cut by basaltic dykes. This is overlain by >500 m of basaltic lavas intruded by rhyolite (Gustafsson, 1992; Burchardt, 2008). The dykes extending from the rhyolitic intrusion at the base feed a ~100 m thick, irregular rhyolitic lava, which caps the basalt unit. Rhyolitic and basaltic intrusions crosscut each other, and indicate the existence of a source magma chamber near the centre of the caldera (Burchardt et al., 2011). The lens-shaped 1-4 m thick Landsendi sill is located on a peninsula east of Njarðvík-Dyrfjöll, surrounded by fractured basaltic lavas (Fig. 2). Its emplacement depth is estimated at 500 m, indicated by the elevation of the coeval subaerial rhyolite lava higher in the sequence (Burchardt, 2008).

3.2 Krafla

The Krafla volcanic complex consists of a central caldera located on the northern rift zone of Iceland, associated with an elongate N-S trending fissure swarm (e.g. Thordarson and Larsen, 2007). Its activity is related to the rifting, with repeated inflation stages and subsidence events (Björnsson et al., 1979). The caldera is filled with basaltic hyaloclastites and lavas, whereas

rhyolitic products are concentrated at and around the caldera rims. The last eruptions were basaltic and occurred between 1975-84 (e.g. Jónasson, 1994).

Hrafninnuhryggur is a ridge of dominantly obsidian near the south-east rim of the Krafla caldera, formed in a small-volume rhyolitic fissure eruption at ~24 ka (Tuffen and Castro, 2009). The ridge is aligned with N-S fissure trend of the rifting area. At the south of the ridge, glacial dissection to ≤ 90 m beneath the syn-eruptive surface reveals a discordant rhyolitic feeder dyke intruding basalts and hyaloclastites that are overlain by small, obsidian-rich lava bodies (Fig. 3).

3.3 Húsafell

Húsafell volcano in west Iceland was active 3–2.3 Ma ago (Saemundsson and Noll 1974), with three phases of silicic volcanism including the emplacement of significant volumes of ignimbrite. Numerous dykes, sheets, domes and vents were emplaced during the final silicic phase. They are extensively dissected in the valleys of Deildargil and Hringgil. These intrusions emplaced at ~500m depth and cut a series of conglomerates, ignimbrites and basaltic lavas (McGowanl, 2016). The selected outcrops are exposed on both sides of the N-S trending Deildargil valley. On the east outcrop, the ~2m thick inclined rhyolitic sheet-like body propagates through conglomerate. On the west outcrop, it follows the lower boundary of a welded ignimbrite overlaying the conglomerate unit (Fig. 4). It also cut as a dyke through a basaltic lava towards the northern end of the area.

4. Comparative results

An overview of the four intrusions is presented in Table 1. In this section, we will first describe the intrusions structure (geometry and lithologies), with each site presented in Figures 2-4, then the rhyolite texture, those vesicles size and shape are described in Figure 5. The features at the intrusion-country rock interfaces are illustrated on Figure 6 and 7, which introduce damages in country rocks. We then individually describe undamaged and damaged materials. Micro-photographs of geotechnical units are in Figure 8 and summary of their description is in Table 2. Quantitative results in terms of rock properties (Fig. 9; Fig. 10) and fractures (Fig. 11) follow rock qualitative descriptions. This section ends by a summary of results.

TABLE 1. DESCRIPTION OF INTRUSIONS

Field site	UTM	Paleodepth (m)	Intrusion type	Dip °	Thickness (m)	Country rock type	Undamaged rock strength (MPa)
Njarðvík-Dyrkjöll - Landsendi outcrop	65°33'55.75N 13°48'58.93W	500	Lens-shaped sill	10-20	1-4	Basalt lava	90
Krafla - Hrafninnuhryggur outcrop	65°41'13.62N 16°43'40.42W	90-40	Steep conduit	80	3-7	Hyaloclastite	15

Húsafell West outcrop	64°41'23.27N 20°57'20.85W	500	Irregular sheet	45 curving to 05	~ 2	Welded ignimbrite	115
Húsafell East outcrop	64°41'25.78N 20°57'16.44W	500	Sill	10	~ 2	Conglomerate	05

Note: Emplacement depth estimated from topography and literature (Burchardt, 2008; Tuffen and Castro, 2009; Mc Gowan, 2016). Undamaged country rock uniaxial compressive strength estimated using our Schmidt hammer data adjusted with reference to values by Eggertsson (2019).

4.1 The intrusions

4.1.1 Landsendi (Njarðvík-Dyrfföll)

Orientation measurements of the contact and vesicles at the Landsendi sill are consistent with a sill propagating towards the NE at a low discordant angle of $<30^\circ$ (Fig.2A). The intrusion does not follow fractures related to regional stress. Zones of high vesicularity are associated with a higher dip in vesicle orientations and located at the sill tip or adjacent to major faults (Fig.2B), suggesting dynamic degassing. The rhyolite at the contact with country rock is colour-banded, reflecting a spectrum of quenching and devitrification-related textures that are parallel to the contact and reflect variable cooling rates (e.g. Tuffen and Castro, 2009), and, potentially, incremental pulses of magma emplacement (McGowan, 2016). A strongly fractured, friable, clay-rich layer is located at the inner marginal zone, between devitrified margins and intrusion core. These platy joints becomes progressively denser towards the coherent rhyolite at the sill core. The intrusion roof is displaced by several sub-vertical faults where deflection of rhyolite flow banding into faults indicates a syn-emplacement occurrence. Near the middle of the outcrop, an additional scree-hidden fault (Fig.2B) corresponds to an elevation difference of a few metres between the southern and the northern sections. The magma feeder system is not visible, but this middle fault could be related to a feeder dyke or inclined sheet, which could have impacted the intrusion geometry with thickening in the central part (laccolith or lopolith; Mathieu et al., 2008; Schmiedel et al., 2017). Sill thickness abruptly decreases towards the tip cavity, which can result from magma propagation involving elastic tensile fractures (LEFM-Barenblatt behaviour; cf. Galland et al., 2018).

4.1.2 Hrafninnuhryggur (Krafla)

We characterise two parts of the Hrafninnuhryggur feeder dyke exposure: (1) its farthest southern extent and deepest dissection (90 m), where the dyke is ~ 2 m thick and cuts through basalt; (2) 150 metres to the north, and dissected to a depth of only 30-50 m, where the ~ 7 -m-thick intrusion penetrated massive to crudely bedded basaltic hyaloclastite and flares upwards and northwards into the columnar-jointed base of the associated lava (Fig. 3). The presence of an overlying ice body at the time of emplacement promoted rapid magma quenching through interactions with meltwater, resulting in a near-completely obsidian body. Micro-crystalline and

/ or devitrified rhyolite is locally and rarely present within the feeder dyke, although predominant in the overlying dyke-fed lava bodies (Fig. 3C; Tuffen and Castro, 2009). Vesicle orientations within the intrusion shows side-by-side opposite directions reflecting complex magma flow dynamics. At the deepest dissection, a layer of hyaloclastite subdivides the intrusion in two sections, highlighting complex internal propagation (Fig. 3C). Dense glass progressively transitions to highly vesicular glass towards the intrusion margins, then to pumice breccia at the contact with country rocks. This breccia consists of fibrous, tube-like pumices (0.1-10 cm), rare lithic clasts (<3 cm) and dense glassy particles (<1 cm; Fig. 7F).

4.1.3 Húsafell

The complex intrusive architecture at Húsafell highlights diverse types of magma emplacement and propagation (Fig.4D). Due to the strong similarity in intrusion dimensions and textures, and to the progressive continuity in orientations, we assume that intrusive segments at Húsafell West, East, and the northern section, are all parts of one single intrusion separated by a scree-buried fault zone (Fig.4A). At the western outcrops, an intrusive finger stalled underneath the rigid layer of welded ignimbrite. Another finger cuts through it, resulting in a step-wise transgressive sill which follows the tuffisite veins. Two metres above the top contact, a >50 cm thick, near-horizontal tuffisite vein cuts friable, less densely-welded ignimbrite and extends over many tens of metres (Fig.4B). A few major faults cut through the valley, displacing many of the studied formations (Fig.4A). The horizontal tuffisite is therefore probably connected with the intrusion at depth, but erosion has removed any evidence for a connection. Quenched margins at the contact are irregular in thickness, especially at the east outcrop where their fingering into the conglomerate follows fine-grained zone and deviates around coarser zones (Fig.4C). We use the northern section to illustrate features that are of better quality than at other localities, although it is not part of outcrops characterised for this study.

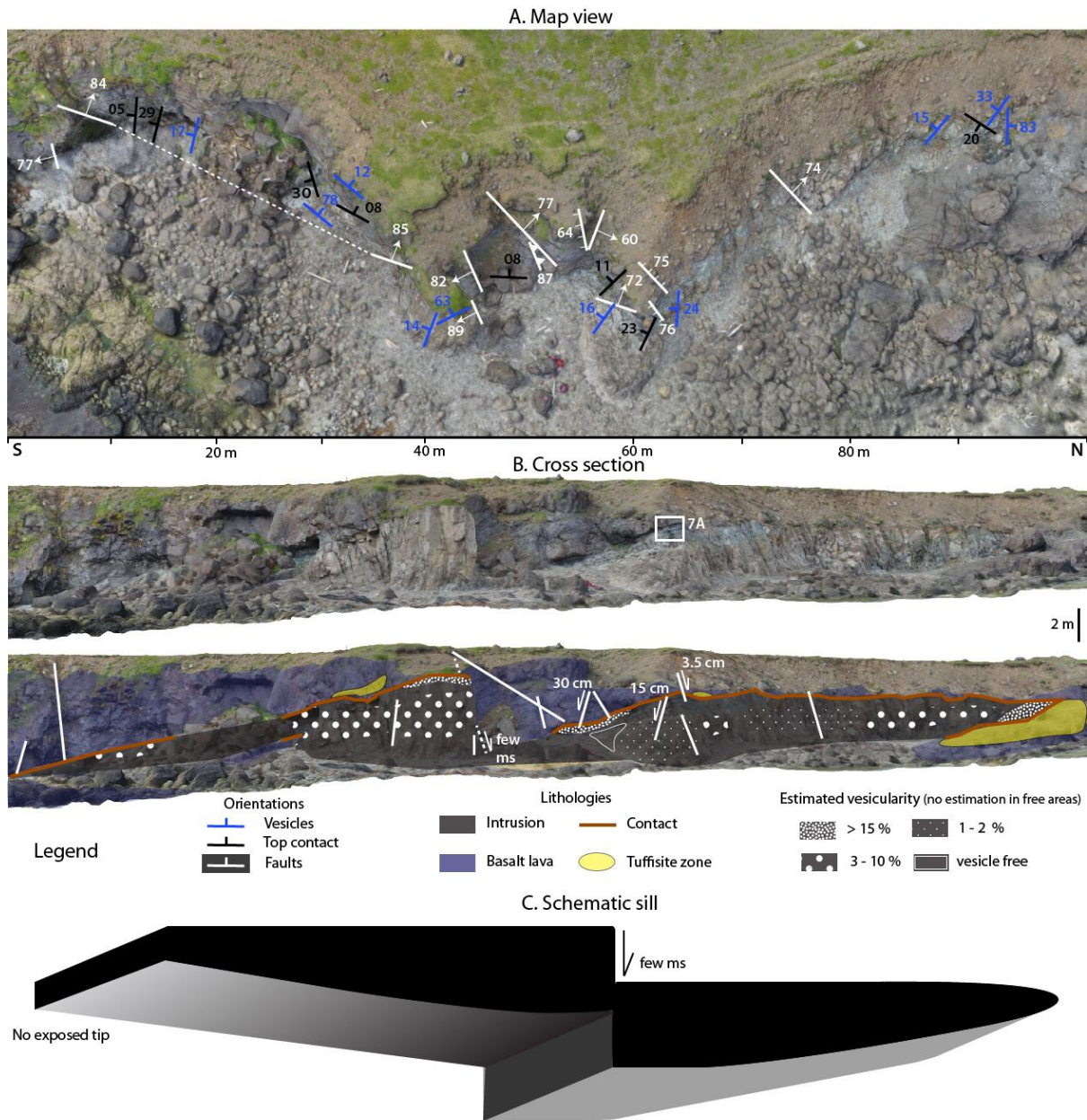


Figure 2. Landsendi 1-4 m thick sill in the *Njarðvík-Dyrfjöll* volcano. A) Map view of the intrusion with orientation of contacts, faults and vesicles. Vesicles in the intrusion core dip at 14-33°, and >63° at intrusion margins. B) Photograph (top) and interpreted cross-section (bottom) of the intrusion with vesicularity estimations, faults and areas containing tuffsites. Location of Fig. 7A is indicated by a white box. Some faults displace the sill by a few cms to >2 m. The cross section corresponds to the area in A, and horizontal-vertical scale difference is caused by the perspective. C) Three-dimensional sketch of the intrusion, based on 3D photogrammetry and field insight into top and bottom contacts. The schematic is simplified to roughly highlight the intrusion shape.

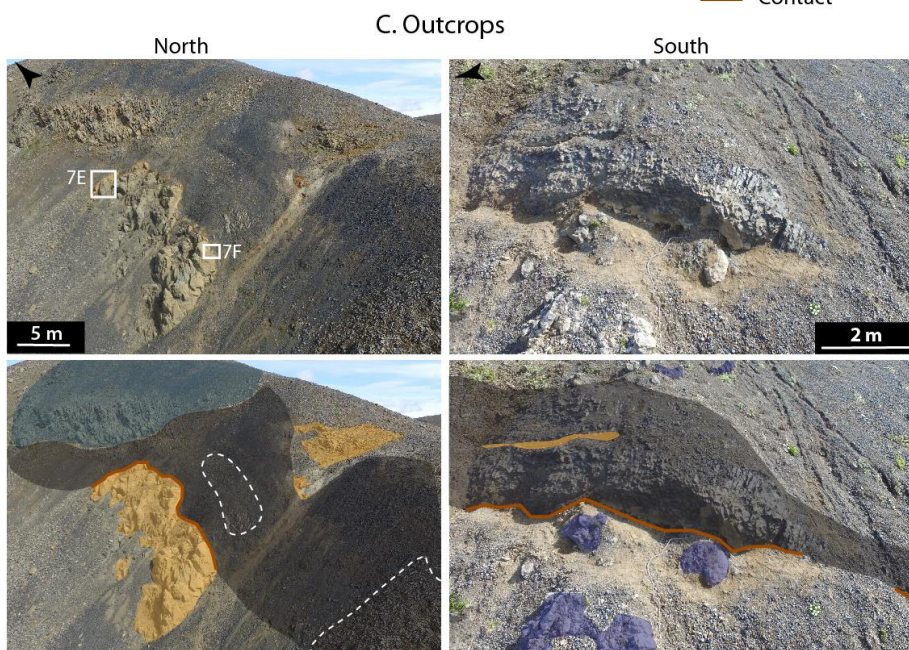
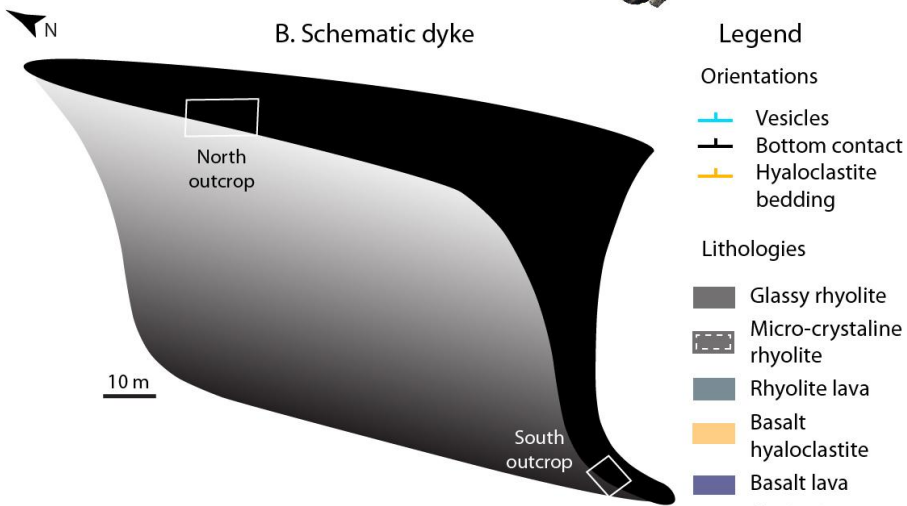
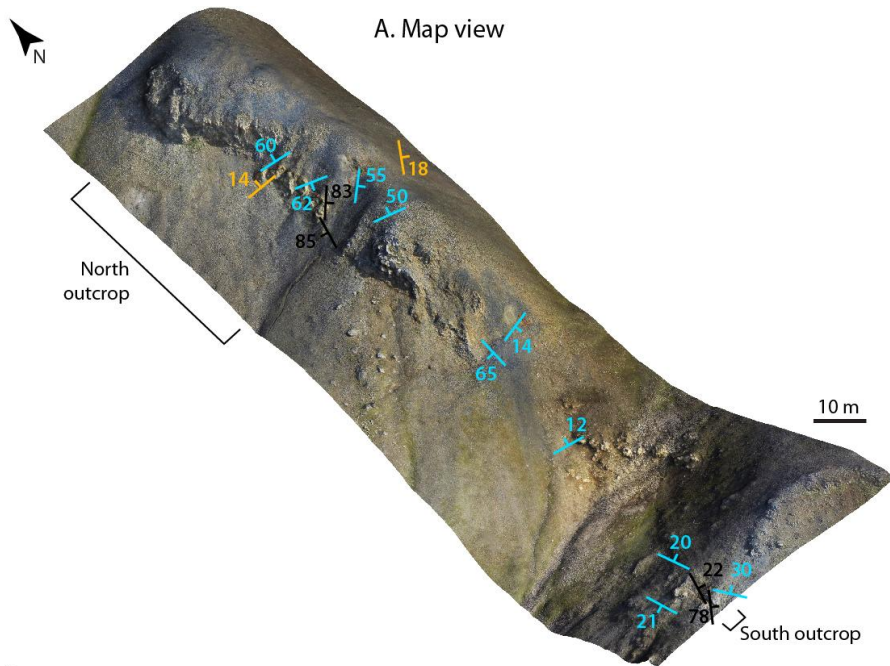


Figure 3. Feeder dyke at the south of Hrafninnuhryggur, Krafla. A) Map view from photogrammetry reconstruction, with orientations of intrusion margins, bedding of hyaloclastite and vesicles within the intrusion. B) 3D representation of the dyke geometry and location of the two outcrops. The scale is roughly similar to the map in A and the sketch is simplified to highlight the intrusive shape. C) Photograph (top) and interpreted (bottom) cross sections of north and south outcrops, with location of pictures for Figs. 7E, 7F. Change in scale from A is caused by perspective effect.

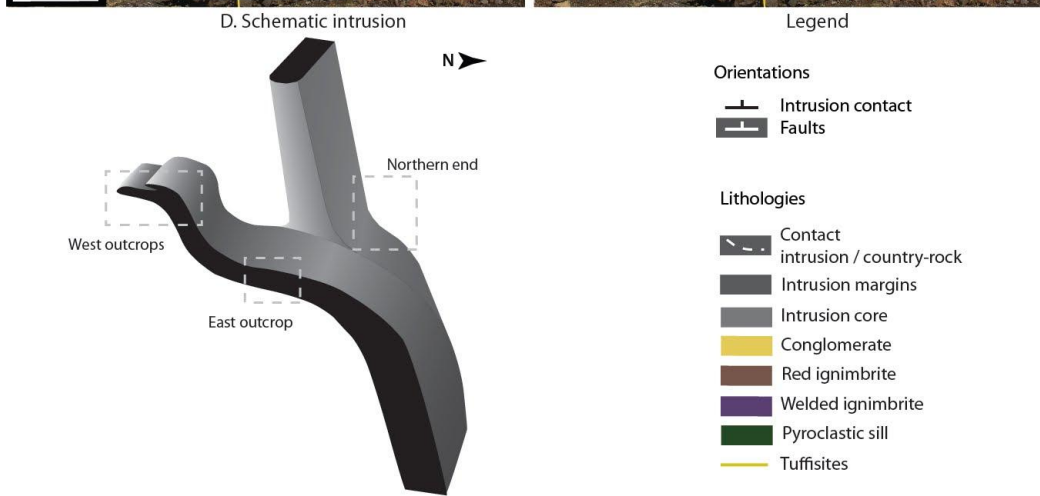
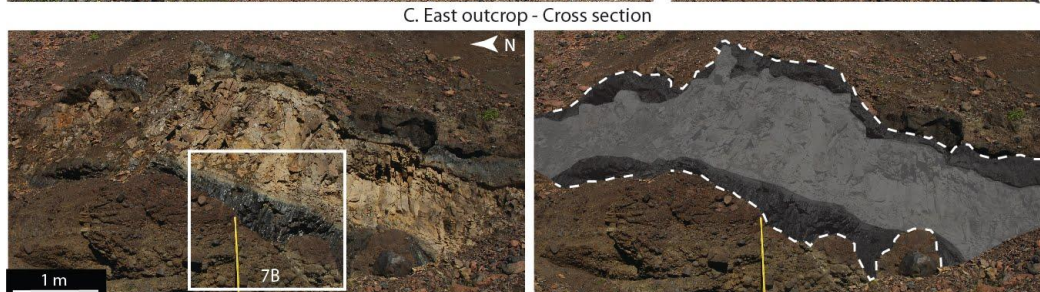
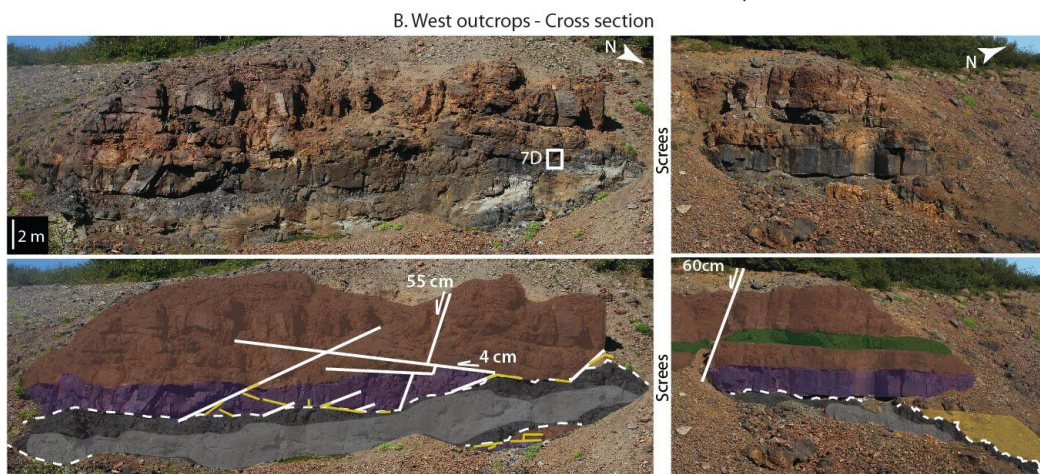
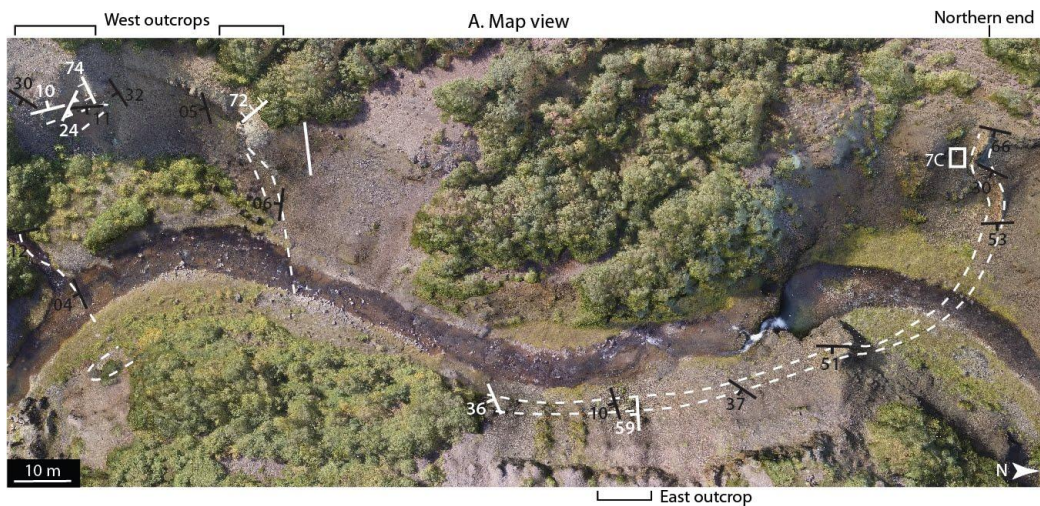


Figure 4. Intrusive system at Deildargil, Húsafell. A) Map view constructed from photogrammetry with orientation of intrusive contacts and faults, location of main outcrops and picture from 7C (white box). B) Photograph (top) and interpreted (bottom) cross section of Húsafell West, with highlighted faults and lithologies, and location of picture from Fig. 7D. 15 m scree-covered metres separate the lateral pictures. C) Photograph (left) and interpreted (right) cross section of rhyolite intrusion through conglomerate at Húsafell East, with location of picture for Fig. 7B. D) 3D geometry of the ~2 m thick intrusion. The sketch is simplified to highlight the shape of the intrusive system. Not to scale.

4.1.4 Textures and vesicles in intrusions

The micro-crystalline core of the intrusions is very fine-grained, consisting of quartz and feldspar with ~1 mm long phenocrysts (Fig. 8C). The transition to glassy quenched margins is sharp (Fig. 7B). The margins exhibit a colour gradient from dark blue or green to black. They consist of dense and nearly crystal-free obsidian (containing ~3% quartz and feldspar phenocrysts), locally devitrified with green amygdales (secondary mineral precipitation within cavities. Figs. 7A; 8B). Quenched margins are cut by fractures that include columnar joints, sub-parallel curvilinear sheet-like fractures and perlitic cracks (Fig. 8A). They alter progressively to clay minerals in zones of high fracture density, and are ultimately replaced by a wet and soft white clay in rills or riverbeds.

Estimated vesicularity in intrusions is ≤5-10 % at cores, increasing towards sill tips and margins. The three field sites show major differences in vesicle size and shape, plotted in Fig. 5 with relative distance from the sill tip for localities of Landsendi and Húsafell West. The lines defined by data for small vesicles are artefact caused by the measurement resolution.

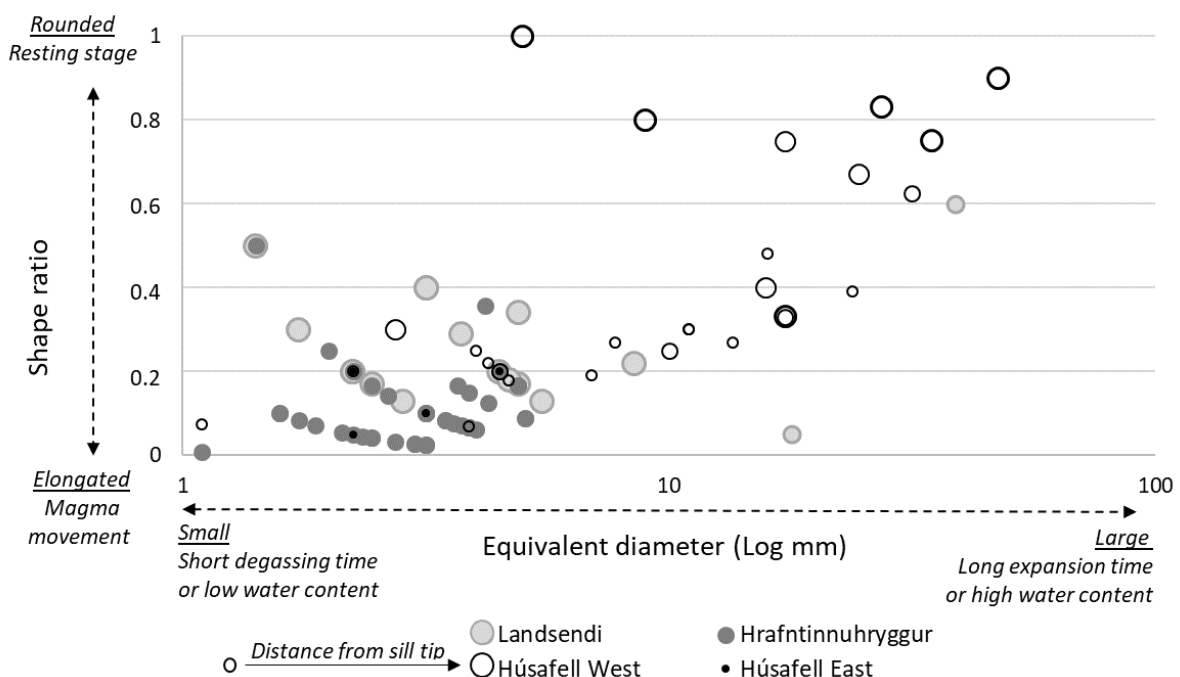


Figure 5. Vesicle size and shape ratio within the intrusions. Each data point represents the largest vesicle in a zone, here all presented together (sill tip, roof, core and bottom of intrusion. c.f. Supplemental material Fig.S1 and Table S3

for location and dimensions). Data from the sill tip at Landsendi are represented with smaller dots and data at Húsafell West are divided into 4 zones: sill tip (smallest dots), 1.5 m away, 5.5 m away and 8.5 m away from the sill tip (largest dots).

At Landsendi, vesicles are small (mean 7 mm in equivalent diameter) and strongly elongated (average shape ratio 0.3). The two largest vesicles were both measured at the sill tip. At Hrafninnuhryggur, vesicles are smaller (mean 3 mm) and have the lowest shape ratio at 0.1 (highly elongate), with decreasing shape ratio for increasing vesicle size. At Húsafell West, vesicles are the largest (12 mm) and have the highest shape ratio of 0.4 (most spherical). It however decreases towards the sill tip, from >0.8 to <0.4 , meaning vesicles are progressively more elongate towards the tip. It also increases with vesicle size, as largest vesicles are the most spherical. At Húsafell East, vesicles are small (3 mm) and elongate (shape ratio <0.2), similar to Hrafninnuhryggur vesicles, although there is no discernible trend.

4.2 The intrusion-country rock interfaces

The intrusion-country rock interfaces (logged for each site on Fig. 6) highlights that rhyolite is systematically chilled at the contact. Fig. 7 shows associated pictures for features of particular interest, and lithologies are pictured in Fig. 8. We observe stratigraphic differences for each site, which can nevertheless be paired: At Landsendi and Húsafell West, tuffisite breccia separates the intrusion from the country rock (Fig. 7D) and tuffisite veins propagate into the country rock (Fig. 7C). At Hrafninnuhryggur and Húsafell East, the rhyolite is directly in contact with the country rock, which shows a colour variation (Fig. 7B,E,F).

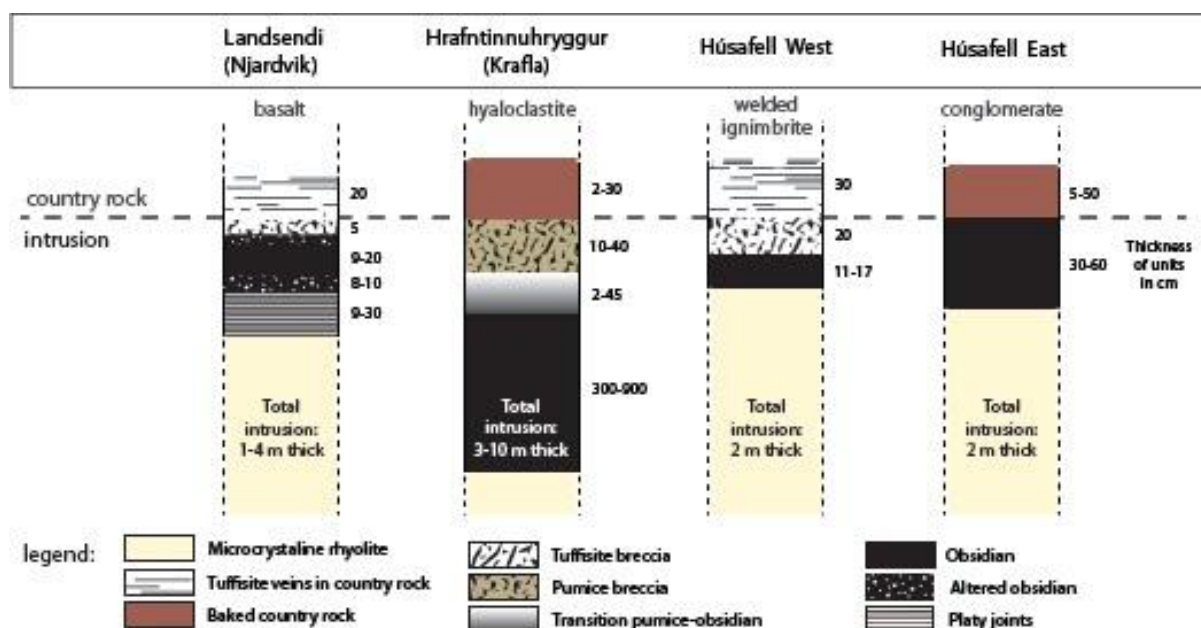


Figure 6. Geological logs of intrusion-country rock interfaces. Thickness given next to each unit is in cm. Country rocks are either baked (hyaloclastite at Hrafninnuhryggur and conglomerate at Húsafell East) or brecciated and fractured

(basalt at Landsendi and welded ignimbrite at Húsafell West). Damage zone thickness is estimated from macro-scale visible indicators, and so are minima as micro-scale alteration is likely more extensive.

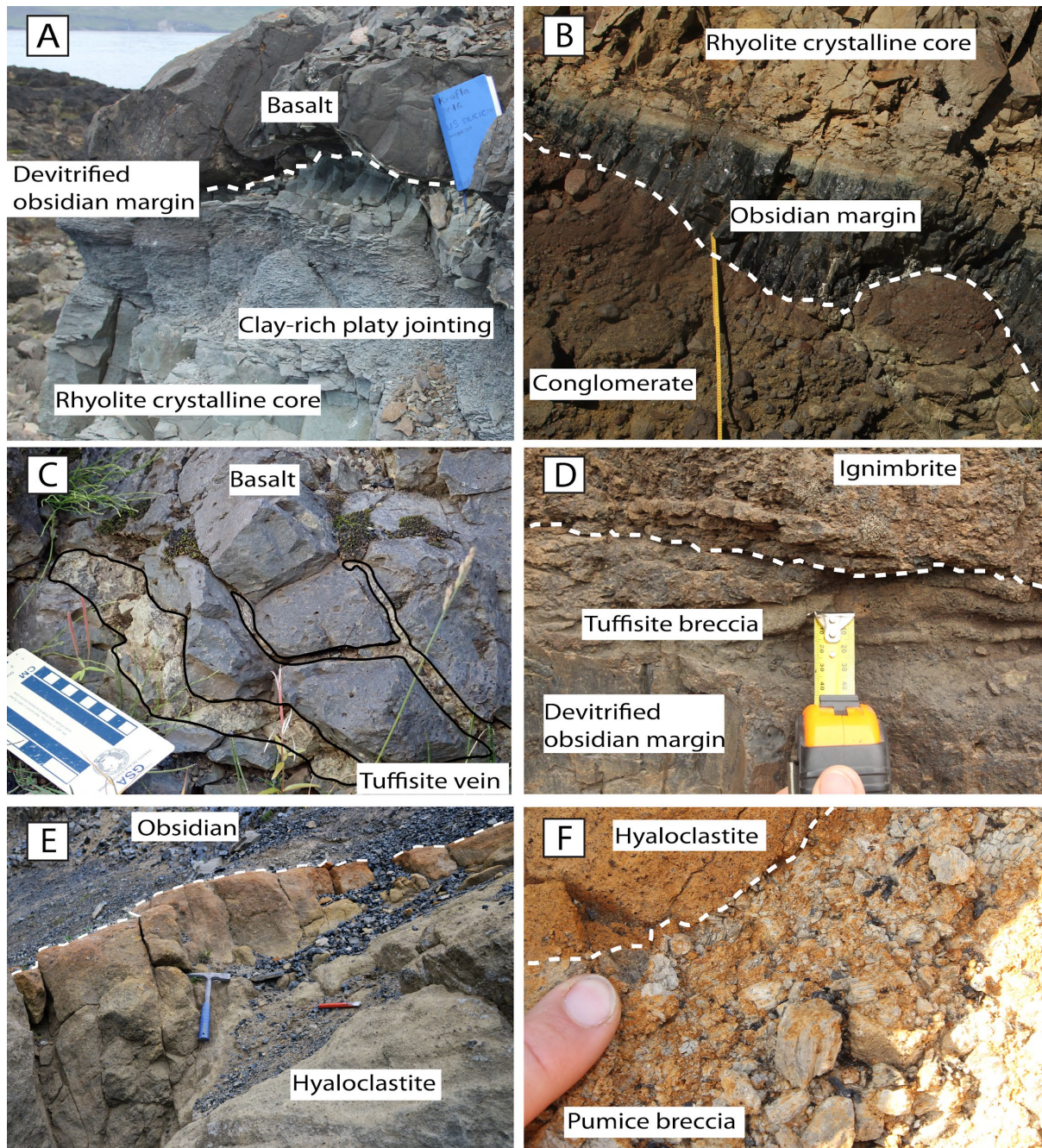


Figure 7. Intrusive materials and country rocks. Contacts are outlined with a white dashed line. A) Platy zone at Landsendi, in between devitrified obsidian and rhyolite core in the intrusion. B) Húsafell East. Directly at the contact, rhyolite is quenched and conglomerate is baked. C) Tuffisite veins (contours in back line) cutting through basalt at the northern end of Húsafell site. D) Húsafell West. Tuffisite breccia between rhyolitic glass and red ignimbrite. E) Hyaloclastite at Hrafninnuhryggur, with colour gradient towards the contact. F) Pumice breccia at the contact with hyaloclastite at Hrafninnuhryggur.

4.2.1 Landsendi – Basalt

Undamaged basalt lava units at Landsendi are exposed in irregular ~3 m-thick sheets. They consist of a poorly vesicular coherent dense core with ~5 mm long feldspar phenocrysts (Fig. 8D). Damaged basaltic lava (Fig. 8H) has vesicles filled with green amygdales. Some fractures are filled with tuffisite veins (similar to Fig. 7C) and in the immediate vicinity of the intrusion, fracture density increases. At the northern sill tip, erosion exposes a ~10 m² surface of underlying basalt covered by an irregular layer of 5 cm thick tuffisite breccia (Fig. 2B). At the intrusion roof, similar breccia appears as local ~20 cm long patches, at one occasion associated with a syn-emplacement fault (Fig. 2B), and tuffisite veins a few millimetres to ~10 cm wide exploit fractures in the basalt. Tuffisite veins are in general filled by predominantly well-sorted and fine-grained (<1mm) material, with occasional coarser (1-5mm), poorly-sorted lenses or layers. Complex depositional structures are present, and most clasts are partially rounded (similar to Fig. 7C). Clasts include lithics derived from the country rocks, juvenile pumices, glass and micro-crystalline rhyolite associated with the intrusion. Tuffisite breccias (Fig. 7D) are coarser-grained equivalents of the tuffisite veins, but are finer-grained, less pumice-rich and more compacted than pumice breccia (Fig. 7F).

4.2.2 Hrafninnuhryggur - Hyaloclastite

At Hrafninnuhryggur, Pleistocene basaltic hyaloclastite was emplaced subglacially and exhibits complex bedding, which may have been deformed or displaced by the intrusion. Bedding irregularity and the rarity of outcrops however prevent any systematic record of orientations (Fig. 3A). Undamaged hyaloclastite is mostly poorly sorted and pale yellowish-brown to grey. Angular clasts include crystalline basalt 1-20 cm in equivalent diameter, and <5 mm clasts are predominantly glassy. Scoria and glass are heterogeneously dispersed in the fine-grained palagonitic matrix (Fig. 8G). Within ~40 cm of the intrusion margin, the altered hyaloclastite displays an orange colour (Figs. 7E; 8K).

4.2.3 Húsafell West - Welded ignimbrite

Undamaged welded ignimbrite from the Deildargil ignimbrite formation is 1.6 m thick, contains 4-5 cm long and >2 cm wide horizontal fiamme, and forms a near-horizontal sheet. The ignimbrite is densely compacted into glass and contains rare 2 mm-long, predominantly feldspathic phenocrysts and many 1-3 cm lithophysae (Fig. 8E). The damaged welded ignimbrite is highly fractured, and these fractures have white alteration haloes <5 mm wide (Fig. 8I). Tuffisite breccias are emplaced along the intrusion margins, forming a <~5 cm thick irregular unit (Fig. 7D). Tuffisite veins cut the ignimbrite, <1 metre from the intrusion (Fig. 7C). One notable sub-horizontal vein cuts friable ignimbrite ~2 m above the intrusion, reaching ~50 cm thick and

exposed over ~60 m. It contains complex sedimentary structures, with interfingering and injection into fragments of friable ignimbritic country rock at the upper and lower vein walls.

4.2.4 Húsafell East – Conglomerate

The contact intrusion-conglomerate at Húsafell East is very sharp and undisturbed by any vein or breccia. The quenched margins follow the country rock irregularities. Undamaged conglomerate is typically massive and poorly-sorted, but locally bedded, with a fine-grained pale grey to yellow matrix. The largest clasts are a few cm in size (Fig. 8F). The damaged conglomerate is more compact and of a browner colour with fractures extending ~10 cm from intrusion margins (Figs. 8J; 7B).

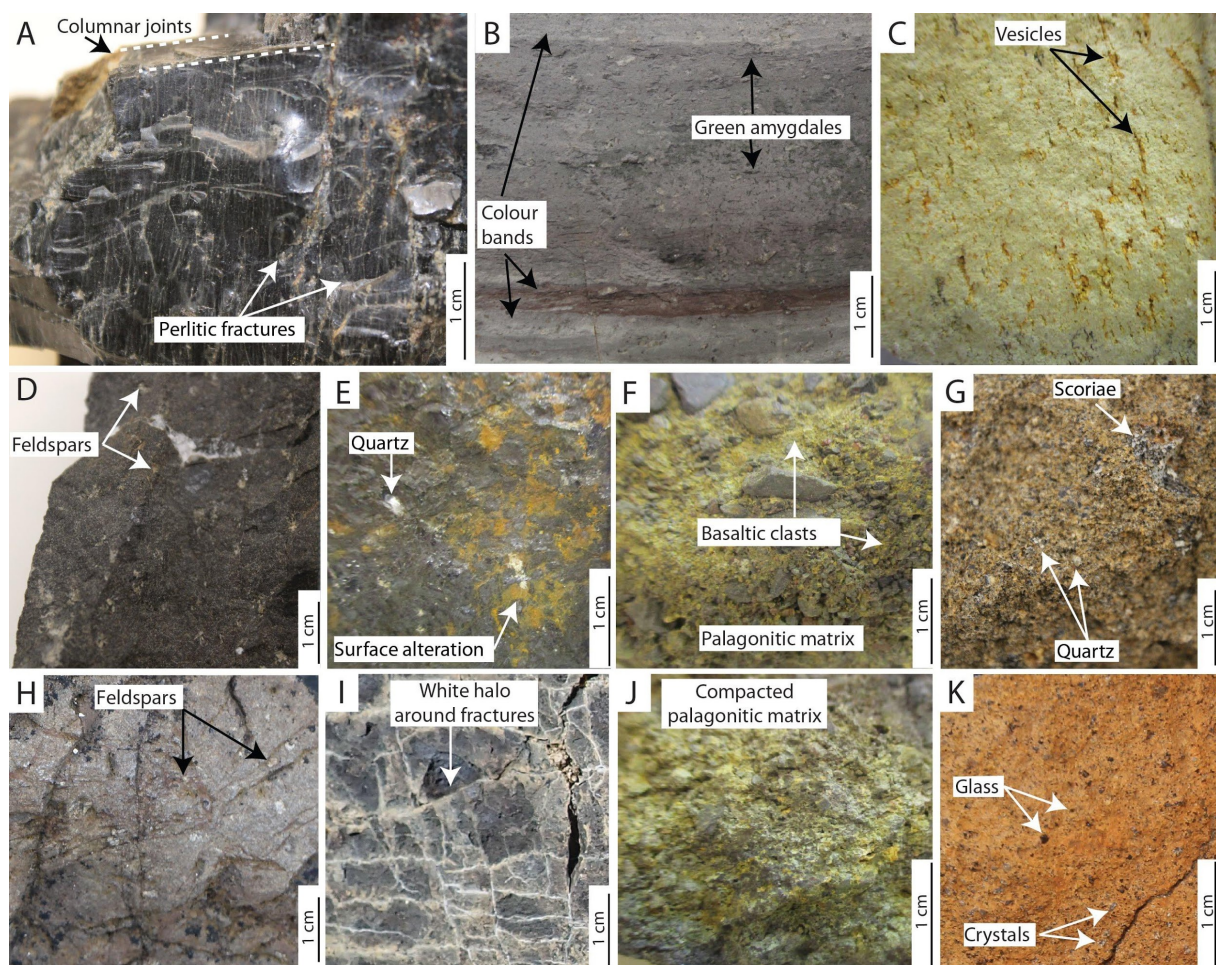


Figure 8. Geotechnical units. A) Obsidian from the glassy margin at Húsafell East. B) Devitrified chilled margins with colour bands at Landsendi. C) Rhyolite core from Landsendi. D) Undamaged basalt lava from Landsendi. E) Undamaged welded ignimbrite at Húsafell West. F) Undamaged conglomerate at Húsafell East. G) Undamaged hyaloclastite at Hrafninnuhryggur with palagonitic matrix. H) Damaged basalt at Landsendi. I) Damaged welded ignimbrite at Húsafell West. J) Damaged conglomerate at Húsafell East. K) Damaged hyaloclastite at Hrafninnuhryggur.

4.3 The impact on country rocks

4.3.1. Geotechnical units

We sort the lithologies into 11 geotechnical units according to the classification by del Potro and Hurliman (2008), illustrated in Figure 8 and briefly described in Table 2: Rhyolite intrusions are subdivided into obsidian margins (Fig.8A), clay-rich altered zones (Fig.8B) and crystalline cores (Fig.8C). Country rocks include undamaged basalt lava (Fig.8D), welded ignimbrite (Fig.8E), conglomerate (Fig.8G), hyaloclastite (Fig.8I) and their damaged equivalents (Fig.8F, 8H, 8J, 8K, respectively).

TABLE 2. GEOTECHNICAL UNITS

Geotechnical unit	Location	Alteration/damage state (sub-unit)	Description
Rhyolite - Crystalline core	All sites	Fresh	Very fine-grained with feldspar phenocrysts (masses of feldspar, SiO ₂ polymorphs, and oxides). Low vesicularity.
Rhyolite - Obsidian margins		Fresh	Near crystal-free perlitic obsidian with variable vesicle content. Spatially variable colour bands including dark blue/green, grey, brown and black.
Rhyolite		Altered	Strongly devitrified and commonly further altered to an assemblage of clay minerals.
Basalt lava	Landsendi	Undamaged	Coherent dense core poorly vesicular, finely crystalline groundmass with feldspar phenocrysts
		Damaged	As above but cut by fractures and tuffisite veins. Vesicles filled with green alteration minerals at Landsendi
Hyaloclastite	Hrafninnuhryggur	Undamaged	Poorly sorted with angular, glassy scoriaceous and crystalline lava clasts cemented in a fine-grained palagonitic matrix. Brown-grey.
		Damaged	Orange colour. Fractures < 20 cm long
Welded ignimbrite	Húsafell West	Undamaged	Densely welded, nearly porosity-free glassy lava-like ignimbrite with distinctive near-horizontal elongated fiamme. Contains 2 mm phenocrysts and 1-3 cm lithophysae.
		Damaged	Highly fractured, with white alteration halo. Cut by tuffisite veins.
Conglomerate	Húsafell East	Undamaged	Massive, poorly-cemented polymictic conglomerate with grey to yellow weakly palagonitised matrix and prominent rounded basaltic clasts. Local better-sorted, bedded lenses.
		Damaged	As above but fractured, with a yellow to brown or red matrix colour

4.3.2 Field assessment of rock properties

Tinyperm and Schmidt hammer measurements of permeability and relative hardness are presented in Figures 9 and 10, respectively. Measurements extend 1.4-3.2 m from the contact into the country rock, with 4-15 measurement points per transect. The permeability increase towards the contact in the damaged basalt and welded ignimbrite is > 1 order of magnitude over ~30 cm, which does not exceed the variability in the undamaged country rock, and is therefore not statistically significant. The variability in undamaged conglomerate and hyaloclastite is smaller (~half an order of magnitude, Fig. 9; Eggertson et al., 2018) and permeabilities decrease towards the intrusion by >1 order of magnitude over 20-40 cm, from $5 \cdot 10^{-13}$ to 10^{-14} and $5 \cdot 10^{-12}$ to 10^{-13} , respectively. These variations thus exceed that of the variability in undamaged rocks and the trends are confirmed by the ANOVA statistical analysis of the results (p-values < 0.04).

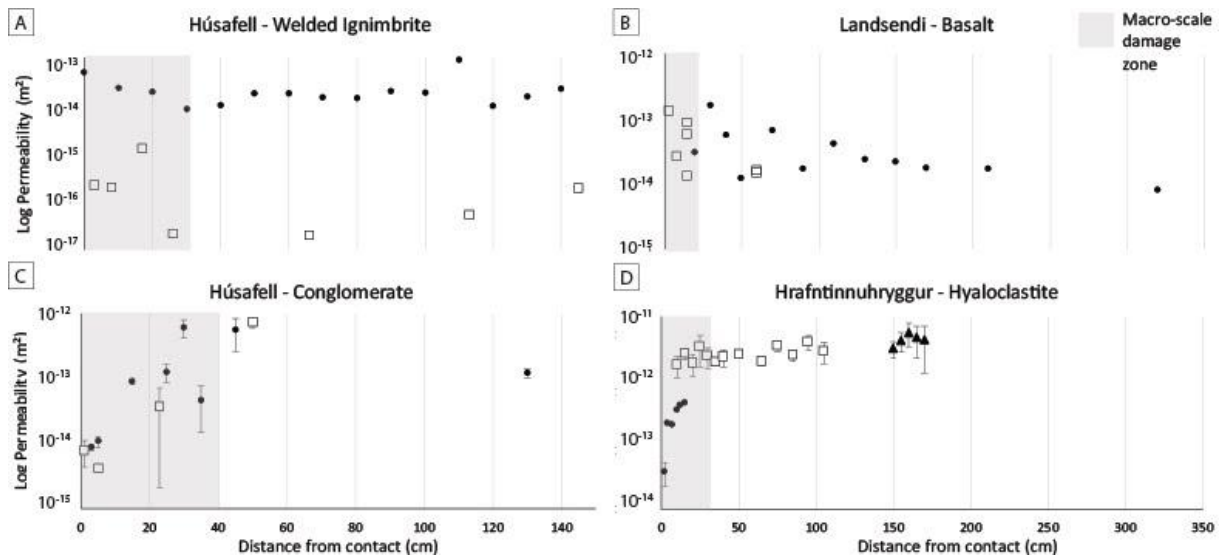


Figure 9. Permeability transects within country rocks. Grey areas show the extent of visible macro-scale damage at the measurement location. Each transect through the same country rock is represented by a different symbol. Error bars are one standard deviation where several measurements were made. Points without error bar were measured once (c.f. Supplemental Material, Table S1). Values have inherent uncertainties of a factor of 1.05 (Brown and Smith, 2013). A) Transects in welded ignimbrite start at the intrusion roof at Húsafell West. These measurement sets were recorded 1 year apart and the 3 orders of magnitude difference between them is likely due to a calibration error. B) Profiles in basalt both start at the intrusion roof. C) Profiles in conglomerate, one from the roof (squares), one from the base of the intrusion (circles). D) Profiles in the hyaloclastite at Hrafninnuhryggur, starting at the intrusion base.

The hardness significantly decreases by a factor >2 towards the intrusion in welded ignimbrite and basalt, with the change initiated at ~ 60 cm and ~ 90 cm distance from the contact, respectively (Fig. 10). This distance is greater than the distance at which macro-scale damages is recorded.

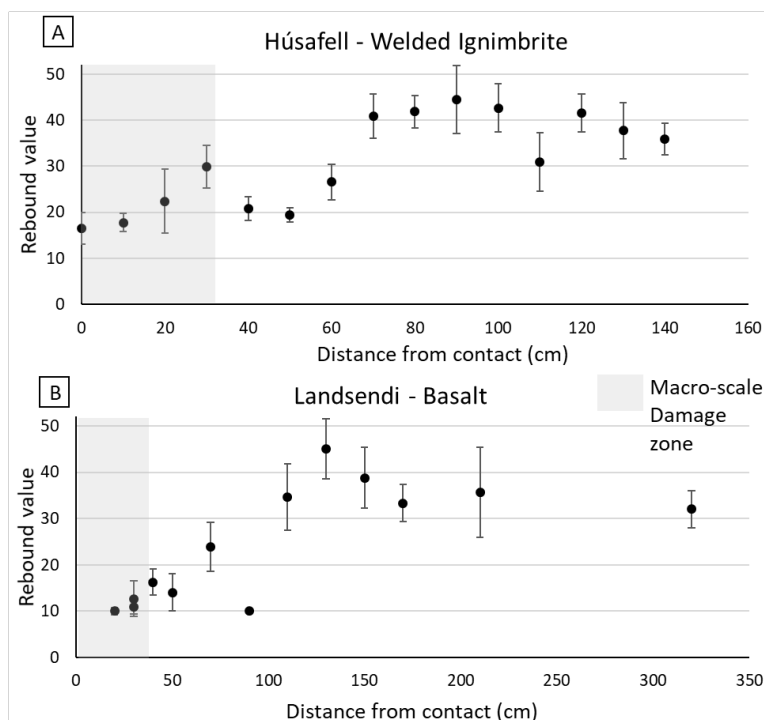


Figure 10. In-situ Schmidt hammer rebound along transects in the country rocks. The rebound value is proportional to rock hardness. Each point on the graph represents the average of ~10 measurements, with error bars representing one standard deviation. Grey areas show the extent of macro-scale damage at the transect location. A) Welded ignimbrite at Húsafell. B) Basalt at Landsendi. Conglomerate and hyaloclastite hardness were too low to be measured using a Schmidt hammer.

4.3.3 Fracture assessment

Fracture density and area at Húsafell are plotted against distance from the contact and averaged per transect and lithology for each outcrop in Figure 11. Data are available in Supplementary material (Fig. S1, Table S2). Changes in fracturing from undamaged to damaged welded ignimbrite and conglomerate are illustrated in Fig. 11C and 11D, respectively. In undamaged country rocks, fracture density is typically 7 fractures per metre within the welded ignimbrite (at ~80 cm from intrusion) and 2 fractures per metre in conglomerate (at ~50 cm from intrusion) (Fig.11A). These values progressively increase towards the contact by a factor of 5-7 (up to 51 and ~10 fractures, respectively). In the damaged zones, the average fracture density systematically exceeds that of the equivalent undamaged rock while the average fracture area is smaller (Fig.11B). Fracture density is higher in undamaged basalt and welded ignimbrite (18 and 22 fractures per metre, respectively) than in undamaged conglomerate and hyaloclastite (5 and 7 fractures per metre).

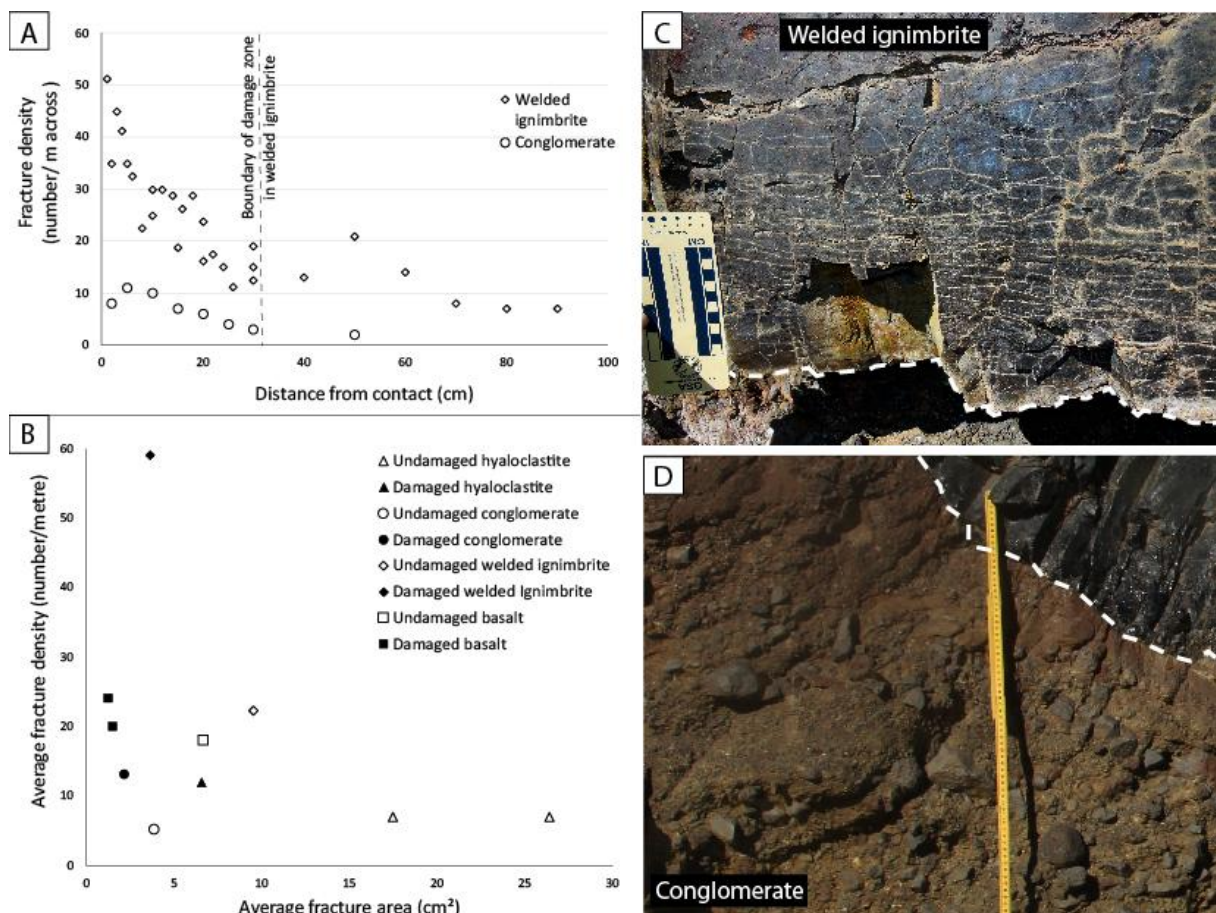


Figure 11. Fracture distribution in country rocks. A) Fracture density at Húsafell with distance from the intrusion. The

dotted line at 30 cm corresponds to the boundary of the macro-scale damage zone in welded ignimbrite. In conglomerate, this zone is irregular, 5-50 cm thick. B) Average fracture density versus average fracture area in undamaged (empty symbols) and damaged country rocks (full symbols). Each data point represents one set of measurements. C) Fractured welded ignimbrite at the contact (white dashed line) with the intrusion at Húsafell West. D) Fractured conglomerate at the contact (white dashed line) with the intrusion at Húsafell East.

4. 4 Summary of the results

At Landsendi, a sill intrudes into competent basalt lava (Fig. 8D) to form an intrusion containing stretched vesicles <15 mm long (Fig. 5) with platy jointing and devitrification of the rhyolite near the margins (Figs. 7A, 8B). The country rock is cut by tuffisite veins (similar to 7C) and by additional macro-fractures at the intrusion interface (Fig. 8H), evidenced by an increase in fracture density (Fig. 11B) and decreased hardness (Fig. 10B).

At Hrafninnuhryggur, a near-surface dyke intrudes through basaltic hyaloclastite to form an obsidian intrusion with highly stretched vesicles (Fig. 5). At the margins, a progressive vesicularity gradient marks the transition towards a pumice breccia (Fig. 7F). The surrounding hyaloclastite is compact and discoloured (Figs. 7E, 8G, 8K), damaged by a few short fractures (Fig. 11B) with matrix permeability reduction of > 1 order of magnitude (Fig. 9D).

At Húsafell, a sill intrudes through conglomerate, deflecting at the base of a basalt lava and arresting at the base of a brittle welded ignimbrite, where the intrusion contains large and rounded vesicles (Fig. 5). The conglomerate at the contact is discoloured (Fig. 7B, 8J, 11D), with a slight increase in fracture density (Fig. 11) and an order of magnitude matrix permeability decrease (Fig. 9C). Where the intrusion encountered the welded ignimbrite and basalt, the interface is surrounded by tuffisite breccia (Fig. 7D) and the country rock is cut by tuffisite veins (Fig. 7C). The number of fractures in the welded ignimbrite increases by ≤ 5 times (Fig. 11) and the hardness decreases by >50 % (Fig. 10A).

5. Discussion

The four intrusions in this study are all rhyolitic in composition, <7 m in thickness and formed during single intrusive events in broadly similar settings and depths within Icelandic central volcanoes. However, they can be differentiated in terms of emplacement mechanism and influence on the surrounding rock, partly reflecting the diverse nature of the intruded country rock.

The mechanical response of the country rocks, together with the stress field, control the intrusive geometry and volume. The heat output to the surrounding country rocks will be primarily controlled by the intrusion thickness, rather than its width and length. However, the orientation

of fractures and contacts (e.g. in dykes or sills) will also influence heat transfer occurring by convection or advection. In addition, internal magmatic processes will further impact heat transfer at the margins and thus country rock alteration.

From their approximate paleo-depth, we assume that water content differs no more than 1 wt % between the intrusions (0.3-0.4 wt. % at Hrafninnuhryggur, Tuffen and Castro, 2009; ~1 wt. % at Húsafell, McGowan, 2016), which correspond to a ~one order magnitude difference in viscosity. This in turn impacts propagation rate and liquidus temperature, which can differ by >100 °C for rhyolitic magmas, impacting the heat input at the interface. Whereas the intrusion at Hrafninnuhryggur fed an eruption, no conclusive evidence demonstrates whether the Landsendi or Húsafell magma was eruptible. However, margins at both of these sites have banding in colour and texture that appears consistent with incremental magma input, which would have induced repeated pulses of heat input to the country rocks that could be distinct from continuous magma flow in the feeder dyke. The variations in vesicle shape ratios highlight different emplacement rates from one intrusion to another, but this comparison is limited by the difference in viscosity, which plays a major role in vesicle response to stress and degassing. The difference in quenched margin thicknesses also indicates variable intrusion margin cooling rate between the sites, with meltwater-assisted cooling at Krafla the most rapid.

As the intrusion thicknesses—the primary factor controlling rock damage—are broadly similar, and magma compositions lie within a restricted rhyolitic range, the macro-scale intrusion impacts on country rock ought to be relatively restricted. In this section we will compare the sites and lithologies to discuss the intrusion emplacement dynamics and their impact on their country rocks.

5.1 Emplacement processes

The intrusions in this study comprise sills, dykes, and conduits: the main types of shallow intrusions at Icelandic central volcanoes. The intrusion morphologies relate to the emplacement mechanisms, with vesicles providing additional information about magma flow direction and degassing, while damage (fracturing and deformation) and alteration record country rock response. The Landsendi sill was laterally emplaced parallel to basaltic lava country rock layers, as evident from its overall morphology, contact relationships, and tip orientation. At Hrafninnuhryggur, an upward propagating dyke widens into a conduit, while the Húsafell intrusions record magma transport in inclined sheets that display characteristics of both dykes and sills.

5.1.1 Landsendi

The tuffisite breccia at the Landsendi sill tip is emplaced against the basaltic country rock (Fig.2B), recording initial emplacement of a fragmental gas-pyroclast mixture during pathway opening. The presence of inner platy-fractured joints (Fig. 7A) is consistent with their formation within a quenching, shearing accommodation zone of outer magma during lateral propagation with high strain rates in the intrusion core. The vesicle population is small yet elongate (average 7 mm in equivalent diameter, 0.3 in shape ratio, Fig. 5), consistent with a brief phase of vesicle growth or a low water content, high shear stresses and minimal relaxation, and thus swift initial emplacement and cooling. At the sill tip, vesicles are larger and have the most extreme values in shape ratio (Fig. 5, the two >10 mm diameter vesicles, with shape ratios of 0.05 and 0.6), indicating a higher variety of vesicle growth processes, such as coalescence and relaxation, locally occurring together.

5.1.2 Hrafninnuhryggur

High glass content and pervasive fracturing in the Hrafninnuhryggur dyke, together with the absence of a platy-fractured zone (Fig.6), indicate rapid quenching, consistent with shallow emplacement under ice. Pumice breccia is found only at this field site, the shallowest of the three, and indicates fragmentation of highly-vesicular initial magma prior to ascent of less-vesicular dyke-filling magma, or prior to foam collapse. The greater vesicle elongation (average shape ratio of 0.1; Fig. 5) suggests higher shear stresses than at the other intrusions, although this can be affected by difference in magma viscosity. It is nevertheless consistent with rapid quenching of ascending magma undergoing shear at high strain rates, with minimal relaxation. The shape ratio decreases with increasing vesicle size (i.e. larger vesicles are more elongated; Fig.5) and could relate to coalescence caused by shearing during magma propagation. The magma could have had a vesicular texture similar to volcanic conduits: large, elongated vesicles on the margins and small rounded vesicles closer to the centre.

5.1.3 Húsafell

The intrusion style at Húsafell particularly reflects the nature of the intruded country rock. In the soft, weak conglomerate on the east side, the rhyolite intrudes irregularly. At the contact with the stronger basalt lava at the northern end, it deflects at the interface before progressing through it. When encountering the stiffer, stronger ignimbrite at Húsafell West, the intrusion forms a bedding-parallel sill periodically injecting pyroclastic material through discontinuities. The intrusion broke through the rigid country rock following the path created by pyroclastic material, propagating as a transgressive sill (Fig. 4). The thick and horizontal tuffisite vein two metres above the intrusion roof is most likely related to the opening stage of the intrusion, when over-pressured gas entered the country rock, creating a magmatic pathway. At Húsafell East, where the intrusion

propagates as a sill through conglomerate, elongated vesicles (<0.2 mean shape ratio, 3mm equivalent diameter, Fig. 5) indicate rapid lateral propagation with high strain rates. At Húsafell West, where the intrusion propagates as an inclined sheet through the ignimbrite, larger vesicles (12 mm in equivalent diameter) could indicate prolonged growth during slower cooling, significant coalescence, and/or a higher magma volatile concentration. Near-spherical vesicle shapes away from the tip (Fig. 5) and absence of platy jointing suggest low shear stresses, or considerable relaxation during protracted cooling. The intrusion into the strong lithology could have triggered magma stalling, creating a static phase of magma relaxation during prolonged cooling that permitted extensive vesicle growth, consistent with the increase in shape ratio with vesicle size (Fig. 5). This sluggish decompression during stalling would lead to low nucleation rates with vesicle growth predominant, and only slight vesicle deformation at zones of highest strain rate close to intrusion margins.

5.2 Country rock response

Intrusive processes have both mechanical and thermal impacts on surrounding country rocks. The undamaged country rock at our field sites consist of both weak, permeable and porous units (hyaloclastite and conglomerate) and strong, less permeable units (basalt and welded ignimbrite) (Table 1; Fig. 9). Geological logs of the contact zone and trends of permeability and hardness in the country rock reveal similarities between the response of hyaloclastite and conglomerate, and between the response of basalt and welded ignimbrite (Fig. 6; Figs. 9 and 10). The differences and similarities in these rock responses to the intrusions highlights the role of the undamaged rock properties. The low strength, high permeability rocks appear to favour hydrothermally-driven alteration, whereas the high strength, low permeability rocks seem initially impacted by mechanical damage. These various rock responses could in turn influence the process of intrusion emplacement.

5.2.1 Rock response by pore occlusion

Hyaloclastite and conglomerate are affected by a colour change (grey-brown to red-orange, Fig.6), pore occlusion with one order of magnitude decrease in matrix permeability (Fig.9C, 9D), a moderate increase in fracture density (7 to 12 and 5 to 13 fractures per metre, respectively; Fig. 11B), and decrease in fracture length and width (18 to 7 cm² and 4 to 2 cm² fracture area, respectively; Fig. 10B).

Thermal alteration is more pervasive in weak country rocks with originally high permeability and porosity. High-temperature fluids readily propagated through the interconnected pore network, with advection and convection expanding the thermally-affected zone. Weak rocks deformed inelastically to accommodate the additional volume of the intrusion and ductile shear failure may

have occurred (as demonstrated in laboratory deformation experiments on altered weak brecciated lava margin in Mordensky et al., 2019). It is unclear if the increase in fracture density arose from new fractures adding to pre-existing discontinuities, which are no longer visible in the vicinity of the intrusions. Compression and contraction could have healed pre-existing discontinuities and opened short tensile fractures, with much of the deformation inelastically accommodated by ductile deformation of the soft country rock. Despite the slight increase in fracture density, there is net pore occlusion and porosity decrease (similar to what was observed in weak, porous, altered andesite by Heap et al., 2015), resulting in decreased matrix permeability. The initial high permeability and porosity of these rocks could favour propagation of high-temperature fluids through the interconnected porous network, with advection and convection expanding the thermally-affected zone. Pore occlusion could result from pore compaction coupled with precipitation of hydrothermal and alteration minerals.

Despite the limitation of this study to the fractures and rock properties, our observations are consistent with pervasive chemical, mineralogical, thermal and fluidal impacts in weak country rocks, similar to that observed in porous brecciated lava margins by Mordensky et al. (2018a).

5.2.2 Rock response by weakening

Basalt and welded ignimbrite are weakened by >50% (Fig. 10), with an associated increase in fracture density (18 to ~22 and 22 to 59 fractures per meter, respectively; Fig.11B), and are crosscut by tuffisite veins. Fractures are narrower and/or shorter in the damage zone (10 to 4 cm² and 7 to 1 cm² in fracture area, respectively; Fig.11B).

Mechanical damage dominates in the originally strong country rocks, with accordingly low permeability and porosity (similar to the mechanical damage in the strong, low permeability dense coherent lava and andesite intrusive in Mordensky et al., 2018a, b). Compared to the hyaloclastite and conglomerate, the fracture density of the welded ignimbrite and the basalt are always higher, revealing brittle deformation behaviour. Pre-existing fractures may have been exploited by gas and fragmented magma at the onset of magma propagation, creating the tuffisite veins (Stasiuk et al., 1996). These veins were then used as a path for coherent magma ascent, which followed the gas and widened the tuffisite veins into intrusions. New fractures were also created, as demonstrated by the lower hardness and high fracture density close to the intrusion (Figs. 10, 11), while matrix permeability was not significantly affected (Figs. 9A, 9B). However, considering the large amount of fractures at the interface, especially in welded ignimbrite, and the significant decrease in hardness in both rocks, the rock mass permeability in these units likely increases towards the intrusions, as observed in originally strong, dense coherent andesite lava and intrusive by Mordensky et al. (2018a).

We have no evidence for chemical, mineralogical or thermal alteration of these strong country rocks, but the intense fracturing suggests the generation of rock mass permeability that is favourable for hydrothermal fluid circulation. Any alteration occurring had a secondary impact compared to mechanical damage.

5.3 Overview and implications

We combine our results and field observations (rock properties, geological logs, contact features, vesicle characteristics) into one conceptual model per field site in Fig. 12, highlighting the emplacement geometry, features indicating intrusive propagation style, and impact on country rocks.

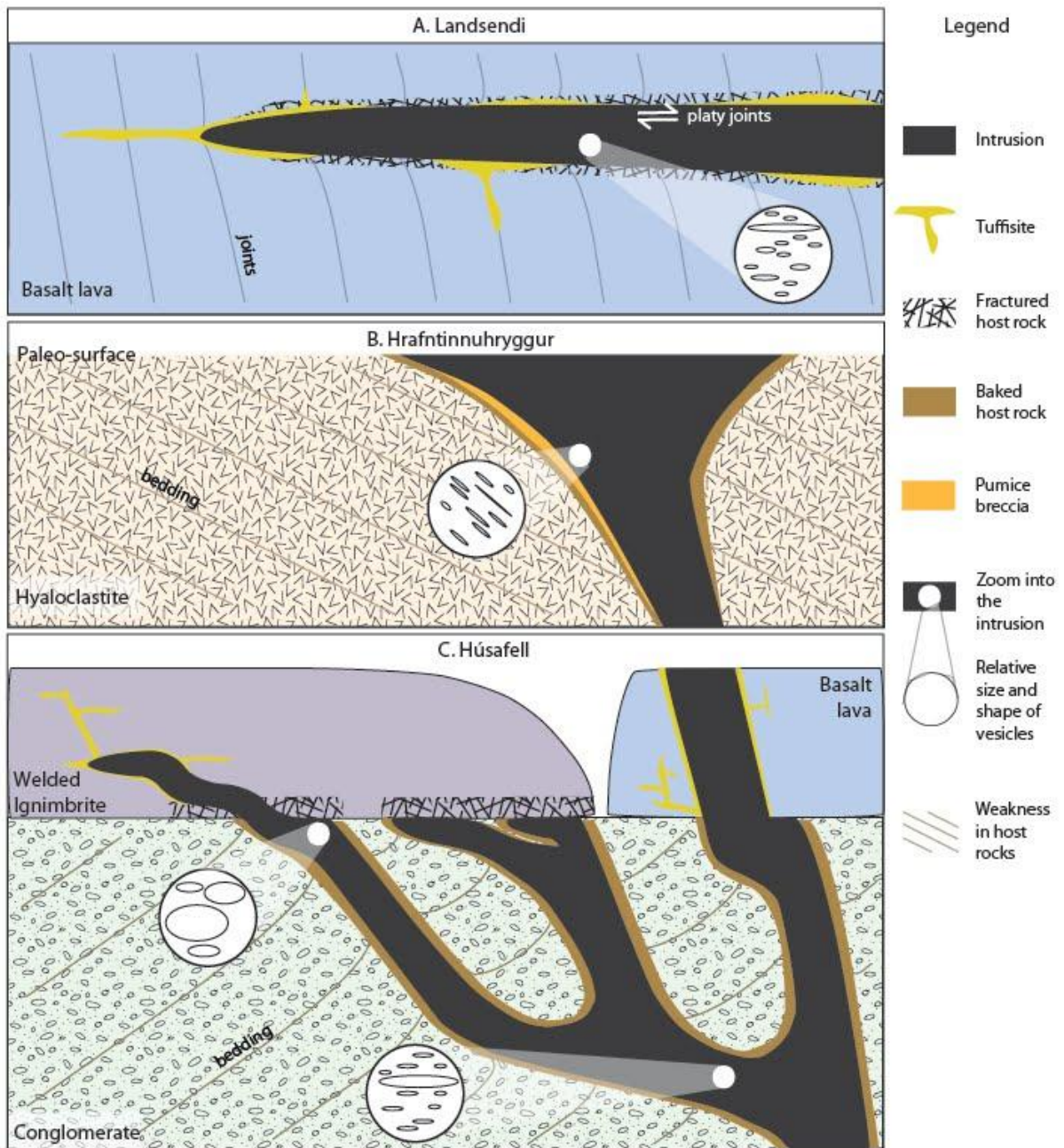


Figure 12. Conceptual models of the intrusions emplaced at 100–500 m depth and their contact features, at the three field sites in Icelandic central volcanoes. Schematic cross-sections are based on results and field observations. Vesicle shapes and relative sizes are indicated within the white circles. Not to scale. A) 1-4 m thick sill at Landsendi. Magma emplaced along a fracture network filled with tuffisite veins. Remnant tuffisite breccia is irregular along the contacts with fractured basalt and a few veins cut through the country rock. Rapid lateral propagation induced high strain rates during magma emplacement, which highly deformed the vesicles. High stress and slow cooling create platy jointing within the intrusion, between the quenched margins and micro-crystalline core. B) 3-7 m thick feeder dyke at Hrafninnuhryggur. Shallow emplacement depth permitted rapid magma decompression, leading to vesiculation, vesicle shear, and formation of pumice at dyke margins. Hyaloclastite at the contact is altered with colour change, pore occlusion and a few tensile fractures. C) 2 m thick intrusion forming a network of dykes and sills at Húsafell. Conglomerate inelastically accommodates magma propagation, resulting in colour change, pore occlusion and opening of small tensile fractures. Within the magma, vesicles are sheared according to the propagation direction. The intrusion is deflected at the base of stronger basalt lava, but cut through it, emplacing along tuffisite breccia in a similar process

to what occurred at Landsendi. Because this section was not characterised in details, variation in fracture population is unknown. The intrusion fractures the base of strong welded ignimbrite, but could have initially failed to intrude it, with repeated attempts creating several intrusive fingers. Magma stalling allows vesicle relaxation into rounded shapes, and the melt eventually propagated into the ignimbrite following tuffisitic patterns.

Transposing the models at deeper emplacement, we would expect the higher surrounding pressure causing lower magma degassing. Vesicularity would thus be lower and material, fluid and gas injection into country rock as tuffisite veins, or magmatic fluids, would be restricted. Country rock fracturing would also be increasingly influenced by lithological pressure and tectonic, and could disappear in favour of ductile deformation below the brittle/ductile transition zone, which occurs at a depth of ~7-9 km in Icelandic crust ([Greenfield and White, 2015](#)). However, hydrothermal reservoirs in Iceland lie significantly shallower than this boundary, which is also deeper than estimated storage depths of Iceland rhyolitic magma (e.g. Weber and Castro 2017). The observed damage zone in country rocks in this study would consequently be representative of active hydrothermal systems, and relevant to Icelandic rhyolitic intrusions.

We propose that gas partitioning related to tuffisite vein and rock fracturing at the onset of magma propagation could possibly prevent the eruption of volatile-depleted magma. At Landsendi, the most vesicular zones are located in the vicinity of the sill tips, tuffisite veins and roof fractures, which can all trigger magma decompression. At Húsafell, magma stalling caused by the encounter with the rigid welded ignimbrite could also be related to a loss in volatiles, as lateral propagation is also aborted. The genetic relationship with the >50 cm thick tuffisite sill, located in country rocks two metres above the intrusion roof, is hidden by vegetation and erosion. If related, such a large syn-eruptive outgassing would have had a major impact on local magma pressure and volatile content. The testing of this hypothesis requires further field investigation.

Damaged and altered country rocks are at the roots of every overlying hydrothermal system. Their rock properties influence the mode of heat transfer and fluid circulation, and thus hydrothermal system architecture. There is no major variation of matrix permeability between different types of damaged country rocks (~1 order of magnitude difference, Fig. 9), but high fracture density in rocks responding by weakening suggests a jump in rock mass permeability. Hydrothermal fluids could propagate in a channelized way through the discontinuities, with a propagation efficiency higher than for rocks responding by pore occlusion. Resulting convection and advection could increase the rate of heat transfer through damage zones, causing a more dynamic hydrothermal system. These more permeable rock masses (as shown in Heap and Kennedy, 2016) could thus make them viable for geothermal fluid extraction, possibly acting as feed zones. We consequently propose that the initial mechanical properties of intrusion-hosting rocks are an important consideration for geothermal exploration and reservoir engineering.

6. Conclusions

This study highlights how country rock response to shallow intrusion of silicic magma can vary depending on its initial properties. Icelandic rhyolitic intrusions were characterised at three field sites and within four country rock lithologies. Results are relevant within the context of Icelandic central volcanoes and shallow magma bodies, above the crustal ductile/brittle transition zone.

At Landsendi, the emplacement of a 1-4 m thick rhyolitic sill into basaltic lava involved a high shear strain rate and rapid lateral propagation, as indicated by tuffisite veins and breccia, platy jointing and elongated vesicles. Basalt at the contact is fractured over ~20 cm and its hardness is decreased by a factor >2.

At Hrafninnuhryggur, Krafla, a shallow, 3-7 m thick eruption-feeding dyke contains highly-elongated vesicles. Upward dyke widening and the presence of pumice breccia reflect the upward acceleration of eruptible magma. Basalt hyaloclastite at the contact is discoloured over <30 cm and fractured, with a decrease in matrix permeability by >1 order of magnitude.

At Húsafell, magma ascent within a complex ~2 m-thick rhyolitic sheet was stalled by encounters with strong welded ignimbrite country rock layers, generating multiple sill tips and large, rounded vesicles in stalled magma that relaxed during prolonged cooling. Welded ignimbrite is highly fractured over 30 cm at the contact and its hardness is decreased by a factor >2. Lateral propagation in the underlying conglomerate resulted in an irregular <50 cm thick discoloured zone in the country rock, crossed by rare short and narrow fractures and corresponding to ~1 order of magnitude decrease in matrix permeability.

We propose a bimodal response behaviour to intrusive processes, based on observed damage and alteration in country rocks which relate to their initial properties, and impact the propagation style:

- Rock response by pore occlusion: in originally weak, porous and highly-permeable conglomerate and hyaloclastite (estimated initial UCS <15), porosity reduces by compaction and/or mineral precipitation, and permeability decreases accordingly by >1 order of magnitude. The inelastic accommodation to magma propagation allows various intrusive geometries to form.
- Rock response by weakening: in initially strong, low-permeability basaltic lava and welded ignimbrite (estimated initial UCS >90), intense fracturing and exploitation of fractures by tuffisite veins weaken the rock by a factor >2. These rocks appear to require accumulation of magmatic pressure with systematic formation of tuffisite veins prior to intrusive emplacement.

Our field observations of intrusion-country rock interactions provide critical information about the process of silicic magma ascent in the shallow crust. Forecasting of silicic magma mobility at caldera complexes, which relies on interpretation of deformation and seismic data, therefore directly relates to the deformation response of intruded country rock. The nature of compaction and fracturing triggered by magmatic intrusion strongly depends on the initial properties of the country rock. This highlights the importance of robust characterisation of the mechanical properties of caldera-filling formations to enable appropriate geophysical data interpretation. Similar knowledge of geothermal reservoir formations will additionally shed useful light on evolving geothermal resources within intruded geothermal systems.

7. Author contributions

The study was devised by ES, BK, HT and MV. Manuscript preparation was led by ES with the inputs and reviews of all the authors. Figures were drafted by ES with contributions from JD. The Njarðvík-Dyrfjöll site was introduced by SB, and Hrafninnuhryggur and Húsafell by HT. All the authors carried out the fieldwork: ES, BK and MV performed scanline transect measurements; ES and HT measured vesicle properties; ES and JD carried out virtual coverage with the remote aircraft combined with high quality hand-camera pictures from BK and HT; Faults were recorded by SB, ES and HT; all the authors contributed to rock properties measurement with the TinyPerm and Schmidt hammer, and to the measurements of features orientation and dimensions. Data analysis was performed by ES and interpretations built with contributions from all the authors. Statistical analysis was conducted by ES.

8. Acknowledgements

The authors thank the National Power Company of Iceland (Landsvirkjun) for the accommodation provided at Krafla. We are also thankful to Felix von Aulock (University of Liverpool, UK) and Einar Bessi Gestsson (Uppsala University and Icelandic Meteorological office) for their assistance on the field, and to the farmers at Njarðvík for kindly giving access to the field sites. This work was supported by the Ministry of Business, Employment and Innovation, New Zealand [grant number E6552]; the Mason Trust funding from the University of Canterbury, New Zealand; and a Royal Society University Research Fellowship to HT.

9. References

- Annen, C. 2017. Factors Affecting the Thickness of Thermal Aureoles. *Frontiers in Earth Science*, 5.
- Albertsson, A., Bjarnason, J. Ö., Gunnarsson, T., Ballzus, C., & Ingason, K., 2003. The Iceland Deep Drilling Project: Fluid Handling, Evaluation, and Utilization, 8.
- Alt, J. C., Honnorez, J., Laverne, C., & Emmermann, R., 1986. Hydrothermal alteration of a 1 km section through the upper oceanic crust, Deep Sea Drilling Project Hole 504B: Mineralogy, chemistry and evolution of seawater-basalt interactions. *Journal of Geophysical Research: Solid Earth*, 91(B10), 10309–10335.
- Arnórsson, S., Axelsson, G., & Saemundsson, K., 2008. Geothermal systems in Iceland. *Jökull*.
- Amaral, P.M., Rosa, L.G., Fernandes, J.C., 1999. Determination of Schmidt rebound hardness consistency in granite. *International Journal of Rock Mechanics and Mining Sciences*, 36, 833 – 837.
- American Society for Testing and Materials, 2001. Standard test method for determination of rock hardness by rebound hammer method. ASTM Standard. 04.09 (D 5873-00).
- Aydin, A. & Basu, A., 2005. The Schmidt hammer in rock material characterization. *Engineering Geology*, 81, 1-14.
- Björnsson, A., Johnsen, G., Sigurdsson, S., Thorbergsson, G., & Tryggvason, E. 1979. Rifting of the plate boundary in north Iceland 1975–1978. *Journal of Geophysical Research: Solid Earth*, 84(B6), 3029–3038.
- Brown, S., & Smith, M., 2013. A transient-flow syringe air permeameter. *Geophysics*, 78(5).
- Burchardt, S., 2008. New insights into the mechanics of sill emplacement provided by field observations of the Njarðvík Sill, Northeast Iceland. *Journal of Volcanology and Geothermal Research*, 173, 280–288.
- Burchardt, S., Tanner, D. C., Krumbholz, M., 2012. The Slaufudalur Pluton, Southeast Iceland - An example of shallow magma emplacement by coupled cauldron subsidence and magmatic stoping. *Geological Society of America Bulletin*, 124, 213-227.
- Burchardt, S., Walter, T. R., & Tuffen, H. (2018). Chapter 4 - Growth of a Volcanic Edifice Through Plumbing System Processes—Volcanic Rift Zones, Magmatic Sheet-Intrusion Swarms and Long-Lived Conduits. In S. Burchardt (Ed.), *Volcanic and Igneous Plumbing Systems*, 89–112.
- Carrigan, C. R., 1986. A two-phase hydrothermal cooling model for shallow intrusions. *Journal of Volcanology and Geothermal Research*, 28(1), 175–192.
- Clemens, J. D., Petford, N. 1999. Granitic melt viscosity and silicic magma dynamics in contrasting tectonic settings. *Journal of the Geological Society*, 156, 1057–1060.
- Conway, C., Townsend, D., Leonard, G. Wilson, C., Calvert, A., & Gamble, J., 2015. Lava-ice interaction on a large composite volcano: a case study from Ruapehu, New Zealand. *Bulletin of Volcanology*, 77.
- Deere, D. U., Miller, R. P., 1966. Engineering classification and index properties for intact rock. Technical report, University of Illinois, Urbana, Illinois, 327p.
- Delaney, P. T., Pollard, D. D., Ziony, J. I., & McKee, E. H., 1986. Field relations between dikes and joints: Emplacement processes and paleostress analysis. *Journal of Geophysical Research: Solid Earth*, 91(B5), 4920–4938.
- Del Potro, R., & Hürlimann, M., 2008. Geotechnical classification and characterisation of materials for stability analyses of large volcanic slopes. *Engineering Geology*, 98(1–2), 1–17.
- Dingwell, D. B., Lavallée, Y., Hess, K.-U., Flaws, A., Marti, J., Nichols, A. R. L., ... Schillinger, B. (2016). Eruptive shearing of tube pumice: pure and simple. *Solid Earth*, 7(5), 1383–1393.

- Eggertsson, G. H., Lavallée, Y., Kendrick, J. E., & Markússon, S. H., 2018. Improving fluid flow in geothermal reservoirs by thermal and mechanical stimulation: The case of Krafla volcano, Iceland. *Journal of Volcanology and Geothermal Research*.
- Eggertsson, G. H., 2019. Constraining mechanical and permeability properties of the Krafla geothermal reservoir, North-East Iceland. PhD thesis, Liverpool University, UK.
- Elders, W. A., Friðleifsson, G. Ó., Zierenberg, R. A., Pope, E. C., Mortensen, A. K., Guðmundsson, Á., ... Schiffman, P., 2011. Origin of a rhyolite that intruded a geothermal well while drilling at the Krafla volcano, Iceland. *Geology*, 39(3), 231–234.
- Farquharson, J., Heap, M. J., Varley, N. R., Baud, P., & Reuschlé, T., 2015. Permeability and porosity relationships of edifice-forming andesites: A combined field and laboratory study. *Journal of Volcanology and Geothermal Research*, 297, 52–68.
- Fisher, R. A. (1925). *Statistical Methods for Research Workers* (Oliver and Boyd).
- Galland, O., Cobbold, P. R., Hallot, E., de Bremond d’Ars, J., Delavaud, G. 2006. Use of vegetable oil and silica powder for scale modelling of magmatic intrusion in a deforming brittle crust. *Earth and Planetary Science Letters*, 243(3–4), 786–804.
- Galland, O., Planke, S., Neumann, E.-R., & Malthe-Sørensen, A., 2009. Experimental modelling of shallow magma emplacement: Application to saucer-shaped intrusions. *Earth and Planetary Science Letters*, 277(3), 373–383.
- Galland, O., Bertelsen, H. S., Eide, C. H., Guldstrand, F., Haug, Ø. T., Leanza, H. A., ... Spacapan, J. B. (2018). Chapter 5 - Storage and Transport of Magma in the Layered Crust—Formation of Sills and Related Flat-Lying Intrusions. In S. Burchardt (Ed.), *Volcanic and Igneous Plumbing Systems*, 113–138.
- Galushkin, Y. I., 1997. Thermal effects of igneous intrusions on maturity of organic matter: A possible mechanism of intrusion. *Organic Geochemistry*, 26(11), 645–658.
- Guðmundsson, A., 1990. Emplacement of dikes, sills and crustal magma chambers at divergent plate boundaries. *Tectonophysics*, 176(3), 257–275.
- Gunnarsson, B., Marsh, B. D., & Taylor, H. P., 1998. Generation of Icelandic rhyolites: silicic lavas from the Torfajökull central volcano. *Journal of Volcanology and Geothermal Research*, 83(1–2), 1–45.
- Hamada, M., Laporte, D., Cluzel, N., Koga, K. T., & Kawamoto, T., 2010. Simulating bubble number density of rhyolitic pumices from Plinian eruptions: constraints from fast decompression experiments. *Bulletin of Volcanology*, 72(6), 735–746.
- Healy, D., Rizzo, R., Duffy, M., Farrell, N. J. C., Hole, M. J., & Muirhead, D., 2018. Field evidence for the lateral emplacement of igneous dykes: Implications for 3D mechanical models and the plumbing beneath fissure eruptions. *Volcanica*, 85–105.
- Heap, M. J., Kennedy, B. M., Pernin, N., Jacquemard, L., Baud, P., Farquharson, J. I., ... Dingwell, D. B., 2015. Mechanical behaviour and failure modes in the Whakaari (White Island volcano) hydrothermal system, New Zealand. *Journal of Volcanology and Geothermal Research*, 295, 26–42.
- Heap, M. J., Kennedy, B. M., 2016. Exploring the scale-dependent permeability of fractured andesite. *Earth and Planetary Science Letters* 447, 139–150.
- Heap, M. J., Violay, M., Wadsworth, F. B., & Vasseur, J., 2017. From rock to magma and back again: The evolution of temperature and deformation mechanism in conduit margin zones. *Earth and Planetary Science Letters*, 463, 92–100.

- Heiken, G., Wohletz, K., & Eichelberger, J., 1988. Fracture fillings and intrusive pyroclasts, Inyo Domes, California. *Journal of Geophysical Research: Solid Earth*, 93(B5), 4335–4350.
- Holness, M. B., 2018. Melt segregation from silicic crystal mushes: a critical appraisal of possible mechanisms and their microstructural record. *Contributions to Mineralogy and Petrology*, 173: 48.
- Huppert, H. E., & Sparks, R. S. J., 1989. Chilled margins in igneous rocks. *Earth and Planetary Science Letters*, 397–405.
- Hutton, D. H. W., 1988. Granite emplacement mechanisms and tectonic controls: inferences from deformation studies. *Earth and Environmental Science Transactions of The Royal Society of Edinburgh*, 79(2–3), 245–255.
- Jónasson, K., 1994. Rhyolite volcanism in the Krafla central volcano, north-east Iceland. *Bulletin of Volcanology*, 56(6–7), 516–528.
- Kavanagh, J. L., Menand, T., & Sparks, R. S. J. (2006). An experimental investigation of sill formation and propagation in layered elastic media. *Earth and Planetary Science Letters*, 245(3), 799–813.
- Kavanagh, J. L., & Sparks, R. S. J., 2011. Insights of dyke emplacement mechanics from detailed 3D dyke thickness datasets. *Journal of the Geological Society*, 168(4), 965–978.
- Kavanagh, J. L. (2018). Mechanisms of Magma Transport in the Upper Crust—Dyking. In S. Burchardt (Ed.), *Volcanic and Igneous Plumbing Systems*, 55–88.
- Kennedy, B. M., Wadsworth, F. B., Vasseur, J., Ian Schipper, C., Mark Jellinek, A., von Aulock, F. W., ... Dingwell, D. B. (2016). Surface tension driven processes densify and retain permeability in magma and lava. *Earth and Planetary Science Letters*, 433, 116–124.
- Krumbholz, M., Hieronymus, C. F., Burchardt, S., Troll, V. R., Tanner, D. C., & Friese, N., 2014. Weibull-distributed dyke thickness reflects probabilistic character of host-rock strength. *Nature Communications*, 5, 3272.
- Lamur, A., Kendrick, J. E., Eggertsson, G. H., Wall, R., Ashworth, J. D., & Lavallée, Y., 2017. The permeability of fractured rocks in pressurised volcanic and geothermal systems. *Scientific Reports*, 7(1).
- Le Corvec, N., Menand, T., & Lindsay, J., 2013. Interaction of ascending magma with pre-existing crustal fractures in monogenetic basaltic volcanism: an experimental approach. *Journal of Geophysical Research*, 118, 968–984.
- Maccaferri, F., Bonafede, M., & Rivalta, E., 2011. A quantitative study of the mechanisms governing dike propagation, dike arrest and sill formation. *Journal of Volcanology and Geothermal Research*, 208(1), 39–50.
- Magnall, N., James, M. R., Tuffen, H., Vye-Brown, C., Schipper, C. I., Castro, J. M., & Davies, A. G., 2019. The origin and evolution of breakouts in a cooling-limited rhyolite lava flow. *Geological Society of America Bulletin*, 131(1–2), 137–154.
- Manga, M., Castro, J., Cashman, K. V., & Loewenberg, M., 1998. Rheology of bubble-bearing magmas. *Journal of Volcanology and Geothermal Research*, 87(1–4), 15–28.
- Mathieu, L., van Wyk de Vries, B., Holohan, E. P., Troll, V. R. 2008. Dykes, cups, saucers and sills: Analogue experiments on magma intrusion into brittle rocks. *Earth and Planetary Science Letters*, 271, 1–13.
- Mattsson, T., Burchardt, S., Almqvist, B. S. G., Ronchin, E. (2018). Syn-Emplacement Fracturing in the Sandfell Laccolith, Eastern Iceland—Implications for Rhyolite Intrusion Growth and Volcanic Hazards. *Frontiers in Earth Science*, 6.

- McGowan, E. M., 2016. Magma emplacement and deformation in rhyolitic dykes: insight into magmatic outgassing. Ph.D Thesis, Lancaster University, UK.
- Miller, J., & Rupert, G. (1997). *Beyond ANOVA: basics of applied statistics*. Chapman and Hall/CRC Texts in Statistical Science.
- Mordensky, S. P., Villeneuve, M. C., Kennedy, B. M., Heap, M. J., Gravley, D. M., Farquharson, J. I., & Reuschlé, T., 2018a. Physical and mechanical property relationships of a shallow intrusion and volcanic host rock, Pinnacle Ridge, Mt. Ruapehu, New Zealand. *Journal of Volcanology and Geothermal Research*, 359, 1–20.
- Mordensky, S. P., Villeneuve, M., Farquharson, J. I., Kennedy, B. M., Heap, M. J., & Gravley, D. M., 2018b. Rock mass properties and edifice strength data from Pinnacle Ridge, Mt. Ruapehu, New Zealand. *Journal of Volcanology and Geothermal Research*, 367.
- Mordensky, S., Heap, M., Kennedy, B., Gilg, H.A., Villeneuve, M., Farquharson, J., Gravley, D., 2019. Influence of alteration on the mechanical behaviour and failure mode of andesite: Implications for shallow seismicity and volcano monitoring. *Bulletin of Volcanology*, accepted.
- Nielsen, G., Maack, R., Gudmundsson, A., & Gunnarsson, G. I., 2000. Completion of Krafla geothermal power plant. *Proceeding World Geothermal Congress*.
- Okumura, S., Nakamura, M., & Tsuchiyama, A., 2006. Shear-induced bubble coalescence in rhyolitic melts with low vesicularity. *Geophysical Research Letters*, 33(20).
- Okumura, S., Nakamura, M., Takeuchi, S., Tsuchiyama, A., Nakano, T., & Uesugi, K., 2009. Magma deformation may induce non-explosive volcanism via degassing through bubble networks. *Earth and Planetary Science Letters*, 281(3), 267–274.
- Papale, P., Neri, A., & Macedonio, G., 1998. The role of magma composition and water content in explosive eruptions: 1. Conduit ascent dynamics. *Journal of Volcanology and Geothermal Research*, 87(1), 75–93.
- Parmentier, E. M., & Schedl, A., 1981. Thermal Aureoles of Igneous Intrusions: Some Possible Indications of Hydrothermal Convective Cooling. *The Journal of Geology*, 89(1), 1–22.
- Paterson, S. R., Fowler, T. K., & Miller, R. B., 1996. Pluton emplacement in arcs: a crustal-scale exchange process. *Earth and Environmental Science Transactions of The Royal Society of Edinburgh*, 87(1–2), 115–123.
- Pennacchioni, G., Di Toro, G., Brack, P., Menegon, L., & Villa, I. M., 2006. Brittle–ductile–brittle deformation during cooling of tonalite (Adamello, Southern Italian Alps). *Tectonophysics*, 427(1), 171–197.
- Pirajno, F., 2008. *Hydrothermal Processes and Mineral Systems*. Springer Science & Business Media.
- Pollard, D. D. (1973). Derivation and evaluation of a mechanical model for sheet intrusions. *Tectonophysics*, 19(3), 233–269.
- Rust, A. C., Manga, M., & Cashman, K. V., 2003. Determining flow type, shear rate and shear stress in magmas from bubble shapes and orientations. *Journal of Volcanology and Geothermal Research*, 122(1–2), 111–132.
- Saemundsson, K., & Noll, H., 1974. K/Ar ages of rocks from Húsafell, Western Iceland, and the development of the Húsafell central volcano. *Jökull*, (24), 40–59.
- Saubin, E., Tuffen, H., Gurioli, L., Owen, J., Castro, J. M., Berlo, K., ... Wehbe, K., 2016. Conduit Dynamics in Transitional Rhyolitic Activity Recorded by Tuffisite Vein Textures from the 2008–2009 Chaitén Eruption. *Frontiers in Earth Science*, 4.
- Schmiedel, T., Galland, O., & Breitzkreuz, C. 2017. Dynamics of Sill and Laccolith Emplacement in the Brittle Crust: Role of Host Rock Strength and Deformation Mode. *Journal of Geophysical Research: Solid Earth*, 122(11), 8860–8871.

- Scott, S., Driesner, T., & Weis, P. 2017. Boiling and condensation of saline geothermal fluids above magmatic intrusions. *Geophysical Research Letters*, 44(4), 1696–1705.
- Senger, K., Buckley, S. J., Chevallier, L., & Tveranger, J., 2014. Fracturing of doleritic intrusions and associated contact zones: Implications for fluid flow in volcanic basins. *Journal of African Earth Science*, 102, 70–85.
- Shea, T., Houghton, B. F., Gurioli, L., Cashman, K. V., Hammer, J. E., Hobden, B. J. 2010. Textural studies of vesicles in volcanic rocks: An integrated methodology. *Journal of Volcanology and Geothermal Research*, 190(3–4), 271–289.
- Sigurdsson, H., 1977. Generation of Icelandic rhyolites by melting of plagiogranites in the oceanic layer. *Nature*, 269(5623), 25–28.
- Siratovich, P. A., Sass, I., Homuth, S., & Bjornsson, A. 2011. Thermal simulation of geothermal reservoirs and laboratory investigation of thermally induced fractures. *Transactions - Geothermal Resources Council*, 35, 1529–1535.
- Sparks, R. S. J., 1978. The dynamics of bubble formation and growth in magmas: A review and analysis. *Journal of Volcanology and Geothermal Research*, 3(1–2), 1–37.
- Spence, D. A., & Turcotte, D. L., 1985. Magma-driven propagation of cracks. *Journal of Geophysical Research: Solid Earth*, 90(B1), 575–580.
- Stasiuk, M. V., Barclay, J., Carroll, M. R., Jaupart, C., Ratté, J. C., Sparks, R. S. J., & Tait, S. R., 1996. Degassing during magma ascent in the Mule Creek vent (USA). *Bulletin of Volcanology*, 58(2–3), 117–130.
- Thordarson, T., & Larsen, G. 2007. Volcanism in Iceland in historical time: Volcano types, eruption styles and eruptive history. *Journal of Geodynamics*, 43, 118–152.
- Toramaru, A., 2014. On the second nucleation of bubbles in magmas under sudden decompression. *Earth and Planetary Science Letters*, 404, 190–199.
- Tuffen, H., & Castro, J. M., 2009. The emplacement of an obsidian dyke through thin ice: Hrafninnuhryggur, Krafla Iceland. *Journal of Volcanology and Geothermal Research*, 185(4), 352–366.
- Tuffen, H., & Dingwell, D. B., 2005. Fault textures in volcanic conduits: evidence for seismic trigger mechanisms during silicic eruptions. *Bulletin of Volcanology*, 67(4), 18.
- von Aulock, F. W., Nichols, A. R. L., Kennedy, B. M., & Oze, C. (2013). Timescales of texture development in a cooling lava dome. *Geochimica et Cosmochimica Acta*, 114, 72–80.
- von Aulock, F. W., Kennedy, B. M., Maksimenko, A., Wadsworth, F. B., & Lavallée, Y., 2017. Outgassing from Open and Closed Magma Foams. *Frontiers in Earth Science*, 5
- Wadsworth, F. B., Witcher, T., Vasseur, J., Dingwell, D. B., & Scheu, B., 2019. When Does Magma Break? In J. Gottsmann, J. Neuberg, & B. Scheu (Eds.), *Volcanic Unrest: From Science to Society*, 171–184.
- Walker, G. P. L., 1966. Acid volcanic rocks in Iceland. *Bulletin of Volcanology*, 29(1), 375–402.
- Walker, G. P. L., 1974. Eruptive Mechanisms in Iceland. In L. Kristjansson (Ed.), *Geodynamics of Iceland and the North Atlantic Area*, 189–201.
- Weidendorfer, D., Mattsson, H. B., & Ulmer, P., 2014. Dynamics of Magma Mixing in Partially Crystallized Magma Chambers: Textural and Petrological Constraints from the Basal Complex of the Austurhorn Intrusion (SE Iceland). *Journal of Petrology*, 55(9), 1865–1903.
- Westrich, H. R., Stockman, H. W., & Eichelberger, J. C. (1988). Degassing of rhyolitic magma during ascent and emplacement. *Journal of Geophysical Research: Solid Earth*, 93(B6), 6503–6511.

Wong, T., & Baud, P. (2012). The brittle-ductile transition in porous rock: A review. *Journal of Structural Geology*, 44, 25–53.

Zaiontz C. (2018). Real Statistics Using Excel. www.real-statistics.com accessed May 2019